

Evolving spike-protein *N*-glycosylation in SARS-CoV-2 variants

Authors

Sabyasachi Baboo^{*1}, Jolene K. Diedrich¹, Jonathan L. Torres², Jeffrey Copps², Bhavya Singh^{1,§}, Patrick T. Garrett¹, Andrew B. Ward², James C. Paulson^{1,4}, John R. Yates III^{*1}

Affiliations

1 Department of Molecular Medicine, The Scripps Research Institute, La Jolla, California 92037, United States

2 Department of Integrative Structural and Computational Biology, The Scripps Research Institute, La Jolla, California 92037, United States

4 Department of Immunology and Microbiology, The Scripps Research Institute, La Jolla, California 92037, United States

§ Present address: Department of Computer Science and Engineering, University of California San Diego, La Jolla 92093, United States

Corresponding Authors

* Sabyasachi Baboo (sbaboo@scripps.edu), John R. Yates III (iyates@scripps.edu)

Keywords

N-glycan, heterogeneity, SARS-CoV-2, COVID-19, spike-protein, variants, proteomics, mass spectrometry, vaccine, virus

Abstract

It has been three years since SARS-CoV-2 emerged and the world plunged into a “once in a century” pandemic. Since then, multiple waves of infection have swept through the human population, led by variants that were able to evade any acquired immunity. The co-evolution of SARS-CoV-2 variants with human immunity provides an excellent opportunity to study the interaction between viral pathogens and their human hosts. The heavily *N*-glycosylated spike-protein of SARS-CoV-2 plays a pivotal role in initiating infection and is the target for host immune response, both of which are impacted by host-installed *N*-glycans. We compared the *N*-glycan landscape of recombinantly expressed, stabilized, soluble spike-protein trimers representing seven of the most prominent SARS-CoV-2 variants and found that *N*-glycan processing is conserved at most sites. However, in multiple variants, processing of *N*-glycans from high mannose- to complex-type is reduced at sites N165, N343 and N616, implicated in spike-protein function.

Introduction

The COVID-19 pandemic caused by SARS-CoV-2 (SARS-2)^{1,2} has highlighted the threat that zoonotic viruses pose to human health and socio-economic sustainability^{3,4}. The current pandemic is the most severe humans have experienced in a century, with a global death toll of 6.9 million and infection of more

than 9.5% of global human population (<https://covid19.who.int/>, <https://www.census.gov/popclock/>). The original SARS-2 strain is believed to have begun as a moderately transmissible virus, infecting its first human host(s) in China in late 2019⁵⁻⁷. Since then, SARS-2 has infected the human population in surges, mutating frequently and evolving into increasingly more transmissible variants^{4,8-10} (**Figure 1A**). Wuhan-Hu-1, the original SARS-2 strain, was the dominant strain throughout 2020, and has since produced 5 variants of concern (VoC), as defined by World Health Organization (WHO): Alpha, Beta, Gamma, Delta, and Omicron¹¹. The Alpha variant was first detected in the United Kingdom, was highly transmissible, and quickly became the most dominant variant outside of South America and Africa from December 2020 until July 2021^{12,13}. Almost simultaneously, Beta was detected in South Africa and became dominant in Africa¹⁴, and Gamma was detected in Brazil and became dominant in South America¹⁵. The highly virulent and transmissible Delta¹⁶ was first detected in India in mid-2021 and became the dominant variant until it was overtaken in January 2022 by the currently dominant Omicron¹⁷. GISAID (<https://gisaid.org/>) followed the spread of 2 WHO-recognized variants of interest (VoI), Mu^{18,19} (first detected in Colombia) and Lambda²⁰ (first detected in Peru), which emerged in 2021 and partially overlapped with Gamma in South America.

Thanks to decades of scientific research devoted to the improvement of vaccine technology and advances in an understanding of the immunology of viral infection (especially that of Corona viruses, Human Immunodeficiency Virus (HIV) and Influenza)²¹⁻²⁹ successful vaccines to counter SARS-2 infection were developed at an unprecedented pace³⁰⁻³⁷. These vaccines were designed against heavily glycosylated spike-protein (S-protein) trimer, commonly known as “spike”, anchored to the lipid-bilayer of the SARS-2 viral envelope^{30,38}. This non-covalently associated trimeric form of spike-protein mediates virus entry by binding to its host cell-surface receptor, human ACE2 (Angiotensin converting enzyme 2)^{39,40}. After fusing with a host cell, SARS-2 replicates its genetic material, and the host’s translation apparatus is hijacked to synthesize viral proteins^{41,42}. The spike-protein is glycosylated with high mannose to complex type *N* (asparagine)-linked glycans at sequons encoded by Asn-X-Thr/Ser or NX(S)T, where $X \neq P$ ($S = \text{serine}$, $T = \text{threonine}$, $P = \text{proline}$)⁴³. Glycans are added co-translationally by *en bloc* transfer from a lipid-containing intermediate to yield $\text{Glc}_3\text{Man}_9\text{GlcNAc}_2\text{-Asn}$. The monomers then fold and assemble into a trimeric spike in the endoplasmic reticulum (ER) lumen⁴⁴⁻⁴⁶. Subsequently, as the spike progresses from ER through the Golgi complex (GC), the *N*-glycans are converted from high mannose type glycans to complex type glycans by a process involving trimming of the outer Glc and Man residues, and addition of ‘complex’ saccharides by terminal glycosyltransferases⁴⁴⁻⁴⁶. The degree of conversion of high mannose to complex type *N*-glycans at each glycosylation site is influenced by the structural dynamics of a glycoprotein and the proximity of other *N*-glycans that can restrict access of the processing enzymes⁴⁷. At most *N*-glycosylation sites on SARS-2 spike-protein, glycans are processed to complex type, while only at a few sites (*e.g.*, N234), minimal processing causes high mannose type glycans to remain.

Interest in site specific glycosylation of the spike-protein stems from the functional significance of these glycans in infection and the host immune response. The opening up of the spike-protein receptor binding domain (RBD) for initiating interaction with ACE2 on host cells, is shown to be regulated by glycans on N122, N165, N234 and N343⁴⁸⁻⁵⁰. In addition, *N*-glycans of viral spike glycoproteins shield the underlying protein structure facilitating escape from host immune responses^{46,51,52}. Thus, for rational design of vaccines capable of offering protection against evolving SARS-2 variants, it is important to assess the *N*-glycan landscape on the SARS-2 spike⁵³⁻⁵⁷. Multiple critical mutations that have appeared on spike-protein of SARS-2 variants, are known to facilitate escape from human immunity^{58,59}, and some of these mutations might be responsible for a change in the *N*-glycan landscape of the spike, partially explaining the immune escape strategies of SARS-2 variants^{9,38}.

Here, we present a systematic evaluation of the *N*-glycan landscape of the spike-protein from the original SARS-2 strain and 7 of its variants (Alpha, Beta, Gamma, Delta, Omicron, Mu, and Lambda). We also evaluated the effect of mutations required to produce soluble spike-protein trimer as effective immunogens. We compare our results with the *N*-glycan landscape of the recombinant spike manufactured by Novavax (NVX-CoV2373), used as a vaccine against SARS-2⁵⁵, which has been recently authorized by United States Food and Drug Administration (US FDA) for emergency use.

Results

Analysis of *N*-glycan landscape on spike-protein

The spike-protein of Wuhan-Hu-1 is 1,273 amino acids long and *N*-glycosylated (we exclusively analyze *N*-glycans in this study) at 22 potential *N*-glycosylation sites (NGS)⁵³ (**Figure 1B**). The spike trimer is comprised of 3 protomers and has an apical broad head consisting of the receptor binding domain (RBD) surrounded by the N-terminal domain (NTD) at its base, and tapers down to a long stalk^{30,49,60} (**Figure 1C**). The spike head of a single spike-protein protomer is >1,100 amino acid long, populated by 8 NGS in NTD, 2 NGS in RBD and another 9 NGS. The 10 NGS in NTD and RBD are some of the most extensively studied glycosylation sites^{48,49,61,62}. The spike stalk consists of <150 amino acids per protomer, populated by only 3 NGS.

We used recombinantly expressed SARS-2 spike (M1-Q1208) in cultured human cells. These proteins lacked the transmembrane (TM) and C-terminal (CT) domains but included C-terminal tags to aid in trimerization and affinity purification. The Furin cleavage site (FCS, S1/S2) was abrogated (682RRAR substituted with 682GSAS) to stabilize the spike (**Figure 1B, Tables S1,S2**). The structural integrity and purity of the spikes in their prefusion state was validated with size-exclusion chromatography (SEC) and negative-stain electron microscopy (NS-EM) (**Figure S1**). We employed a DeGlyPHER⁶³ approach that uses sequential deglycosylation followed by bottom-up mass spectrometry (MS)-based proteomics to resolve the site-specific *N*-glycan heterogeneity on spikes from 7 SARS-2 variants and the Novavax full-length spike-protein (NVX-CoV2373; expressed in Sf9 cells *i.e.*, insect cells) and compared them with the Wuhan-Hu-1. DeGlyPHER allowed us to broadly resolve the abundance of high-mannose (including hybrid) and complex glycans at each NGS and to estimate glycan unoccupancy⁶⁴.

Original SARS-CoV-2 strain/Wuhan-Hu-1

Wuhan-Hu-1 is believed to have jumped from an undetermined animal reservoir(s) to humans at the end of 2019^{5,6}, and its spike is one of the most studied protein structures in recent times⁶⁰. Most of the 22 NGS on spike-protein are predominantly complex type; only N122, N234, N603, N709, N717, N801 and N1074 show substantially more high mannose-type glycans (**Figure 2A**). This glycan distribution corroborates earlier reports that employed traditional glycoproteomic approaches for analysis of this glycoprotein^{53,65}. We analyzed 3 different versions of the spike-protein that were mutated to stabilize the immunogen in its prefusion state (**Figure 1B**). The first version, 2P, contains 2 residues (K986 and V987) that were substituted to proline and this mutant is used for most of the currently authorized SARS-2 vaccines^{26,55}. The second version, 6P (or HexaPro), has 4 additional proline substitutions at positions F817, A892, A899, and A942 which help with stability and increase protein yield⁶⁶. The third version, 6P-Mut7, adds an additional interprotomer disulfide bridge at positions V705C/T883C, thus further stabilizing the immunogen while keeping the RBD flexible⁶⁷. When we compared the glycan distribution pattern between 2P, 6P, and 6P-Mut7, the 6P/6P-Mut7 mutants exhibited a significantly higher proportion of high mannose glycans at N603, N801 and N1074 relative to the 2P mutant, but there were no statistically significant differences between 6P and 6P-Mut7 mutants, (**Figure 2B,C,D**). We sampled considerably fewer peptides mapping to N709 and N717 in 6P-Mut7 than in 2P/6P mutants of Wuhan-Hu-1, and this trend was also observed for spikes from other SARS-2 variants (**Figure S2A**). The stalk of the spike is highly conserved across Beta-coronaviruses⁶⁸, and thus it provides a promising target for immune intervention⁶⁹. The 3 NGS (N1158, N1173 and N1194) on the stalk of the SARS-2 spike are fully occupied by complex glycans in all the variants (**Figure 3A**). Complex glycans on these 3 NGS are known to massively shield the stalk at the flexible hinges that are prominent epitopes for immune recognition by antibodies^{49,70}. Their conservation across evolving SARS-2 variants suggests that there is no apparent selection pressure from host immunity to modify the glycan shield around the stalk.

SARS-CoV-2 variants of concern/interest

For the first year of the COVID-19 pandemic the only mutation acquired by the SARS-2 spike-protein that could be positively selected to establish stable VoC/I was D614G^{9,71}. The N501Y mutation in the spike RBD established 3 new VoCs, Alpha (501Y.V1 or B.1.1.7 or 20I), Beta (501Y.V2 or B.1.351 or 20H) and Gamma (501Y.V3 or P.1 or 20J)⁷². N501Y, which is reported to enhance binding affinity of spike RBD to human ACE2, is shared by Alpha, Beta and Gamma⁷³. The other spike RBD mutations include E484K on

both Beta and Gamma, and K417N on Beta and K417T on Gamma. The spike NTD mutations on Alpha (del69-70 and del144), Beta (L18F, D80A, D215G and del242-244) and Gamma (L18F, T20N, P26S, D138Y and R190S) are also known to affect neutralization⁷⁴. None of the mutations in the Alpha or Beta resulted in gain or loss of an NGS, but there were notable changes in glycan processing at several NGS. In the Alpha spike-protein, there were significantly more complex glycans at N122, and more high mannose glycans at N616 (**Figure 3A**). In the Beta spike, there were more high mannose glycans at N165 and N616 (**Figure 3A**). The biggest changes in glycosylation occur in the Gamma spike-protein. Two of mutations resulted in a gain of NGS, T20N creating N20, and R190S creating N188. In the Gamma spike-protein (**Figure 3A**), the new NGS at N20 contained predominantly complex type glycans, and this new NGS had an impact on the adjacent N17 NGS which was largely unoccupied. Moreover, the newly created NGS at N188 is close to N17 and N20 and had largely high mannose glycans. In contrast, glycan composition at N603 and N801 shifted significantly to complex type glycans.

The Delta VoC (B.1.617.2 or 21A) emerged in 2021, spreading globally and replacing the predominance of 501Y lineage¹⁶. D614G is retained in the Delta spike-protein as well. In the Delta spike-protein, T19R mutation in NTD caused the loss of N17 NGS. There was a significant shift to high mannose glycans at N165 and N616 in both 6P and 6P-Mut7, and additionally at N343 in only 6P version. (**Figures 3A;4A,C**).

The Omicron VoC (B.1.1.529 or 21M) replaced the Delta and spread globally in 2022, and Omicron subvariants still dominate¹⁷. The Omicron spike-protein hosts at least 33 mutations, none of which caused gain or loss of any NGS (**Figure 1B**) (though the newer Omicron subvariants are missing N17⁷⁵). D614G is retained in the Omicron spike-protein. Despite this large number of mutations, when we compared the Omicron variant spike to spike from Wuhan-Hu-1 (**Figure 3A,4B,C**), there was no significant shift in site-specific glycan processing. However, we note a shift from high mannose to complex glycans at N122 and *vice-versa* at N165. Additionally, we observed higher unoccupancy at N149 and N657.

The spread of Mu (B.1.1.621 or 21H) and Lambda (C.37 or 21G) Vols was limited to South America^{18,19}. The Mu spike-protein hosts 10 mutations while Lambda spike-protein hosts 7 mutations, the D614G mutation is retained in both (**Figure 1B**), and include some of the known mutations that help SARS-2 escape neutralization^{18,19}. In the Mu spike-protein, there was a significant shift to high mannose glycans at N165, N343 and N616, while glycan unoccupancy increased significantly at N149 (**Figure 3A**). In the Lambda spike-protein, T76I mutation in NTD caused the loss of N74 NGS and there was a significant shift to high mannose glycans only at N1098, though a similar trend was observed at N165 and N343 also (**Figure 3A**).

S2-protein

The post-fusion S2-protein structure that extends from the CT at its base to fusion peptide (FP) (or beyond if S2' cleavage has not occurred) at the top^{76,77}, hosts 3 stalk NGS (N1158, N1173 and N1194) in addition to the 5 NGS (N709, N717, N801, N1074, N1098 and N1134) that are structurally conserved in SARS-CoV⁷⁸. The 5 NGS from N1098 to N1194 are spaced at almost regular intervals of 40Å^{76,77}, suggesting that glycans at these NGS and at N1074 (assuming S2' cleavage) are involved in "caging" the degrees of freedom of the stalk when the viral and host membranes are undergoing fusion⁷⁹. We observed an increase in high mannose glycans at N1098 in the 6P/6P-Mut7 versions versus the 2P version of the Wuhan-Hu-1 virus. This increase is observed in most variants we studied, with the increase being statistically significant in Lambda (**Figure 3A**). Glycans anchored to N1098 on the apical rim of the post-fusion S2-protein^{76,77} could be important determinants of SARS-2's infectivity, as observed in bronchial cells expressing ACE2 when N1098 is occupied with high-mannose *N*-glycans⁸⁰. In this post-fusion S2-protein structure, N1074, N709 and N717 sit just below the apical rim as it extends into the Connecting domain (CD) that hosts N1134^{76,77}. We observed a significant increase in high mannose glycans at N1074 in 6P/6P-Mut7 variant versus the 2P version of the original strain, and this is maintained in most variants studied (**Figure 3A**). Across all variants we studied, glycans decorating N1134 are mostly complex type (**Figure S2B**), although sparse peptide sampling in this region of 6P/6P-Mut7 precludes us from reading too much into this finding (**Figure S2A**). This sparse sampling may be attributable to structural constraints that limit protease access since we avoid harsh denaturants in our sample preparation. Alternatively, these peptides might have reduced ionization in the mass spectrometer⁶³.

NTD

NTD, which forms a whorl around the RBD, has 8 NGS (N17, N61, N74, N122, N149, N165, N234 and N282), the most of any of the structural domains in SARS-2 spike. Five of these NGS (N17, N61, N74, N234 and N282) have highly conserved glycan distributions across variants (**Figure 3A**). Glycans at N17 are difficult to resolve on the spike structure using cryo-EM since it is in the N-terminal unstructured region⁷⁰, except when stabilized by antibodies^{60,62}. N17 is fully occupied by complex glycans (**Figure 3A**), and this trend is conserved across all variants except Gamma, where it is mostly unoccupied, and in Delta and newer subvariants of Omicron, where it is absent⁷⁵. In Gamma, the newly created N20 is known to be glycosylated and exterior to N17 on the N1 loop^{62,81-83}, thus explaining why we observe it to be fully occupied by complex glycans, functionally replacing the adjacent N17. N17, along with N74, N122 and N149 border a multi-epitope “neutralization supersite” on NTD^{62,84}. Absence of N17 in Delta is known to reduce neutralization by antibodies^{81,84,85} and absence of N74 (on N2 loop) in Lambda is known to increase infectivity (the spike-protein we used for Lambda did not include the new N254 NGS in N5 loop which is associated with reduced neutralization by antibodies⁸⁶⁻⁸⁸). N74 is fully occupied by high mannose glycans across all variants except Lambda, where it is absent (**Figure 3A**). N122 is mostly occupied by high mannose glycans across variants, except in Alpha where N122 is significantly more occupied by complex glycans (**Figure 3A**). N122 and N165 are proposed to affect an “RBD-up” conformation⁵⁰. When the spike is in an “RBD-up” conformation³⁰, glycans on N122 are predicted to significantly clash with the highly neutralizing S309 monoclonal antibody binding to its epitope in the “open” RBD. However, its binding is not expected to be affected^{89,90}; indeed, no significant loss in neutralization of Alpha by S309 has been reported^{91,92}, even though we see a shift in the type of glycans on N122 compared to Wuhan-Hu-1 (**Figure 3A**). We found N149 (on surface-accessible N3 loop) to be mostly occupied by complex glycans (**Figure 3A**). When these glycans include GlcNAc₂Man₃, N149 is reported to interact with host cell-surface lectin receptors, enhancing ACE2/spike-protein interaction in lung tissue and consequently driving cell-fusion and syncytia formation that is known to facilitate infection^{93,94}. We observed that N149 is almost completely occupied by glycans in variants where the N3 loop is not mutated (Beta and Lambda), while the glycan unoccupancy at N149 is most significant on Mu (**Figure 3A**). The glycosylation pattern on N165 shifts from almost completely complex type in Wuhan-Hu-1 virus to high mannose glycans in all variants except Alpha and Gamma (**Figure 3A**). The inferred steric occlusion of N165 in most variants (the shift being highest in Delta) is highly relevant given the role of glycans at N165 and N234 in modulating conformational transitions of RBD and its stabilization in an “up” conformation and the RBM (receptor binding motif) is shielded in a “down” conformation^{49,95}. The near-complete occupancy at N234 with high mannose glycans and at N282 with complex glycans is conserved across all variants we studied (**Figure 3A**), with N282 strategically positioned in close proximity to the FP⁶¹ and also implicated in formation of dimeric spike-trimers⁵⁵. In the Gamma variant only, N188 is at the C-terminal edge of the N4 loop, and we find it to be mostly occupied with high mannose glycans (**Figure 3A**), which are reported to increase the glycan shielding effect⁹⁶.

RBD

RBD, which physically interacts with ACE2 and initiates infection, hosts only 2 NGS (N331 and N343). Even in the heavily mutated RBD of Omicron (15 mutations), N331 and N343 are conserved and no new NGS arise. However, some emerging mutations in recent Omicron XBB subvariants affect known N-glycosylation sites and/or create new ones (<https://gisaid.org/hcov19-mutation-dashboard/>) on spike-protein⁹⁷. K529N mutation in Omicron XBB.1.5 subvariant spike-protein RBD creates a new glycosylation site at the RBD-hinge, an otherwise conserved region⁹⁸, close to N331, and its glycosylation can potentially regulate RBD “up/down” dynamics and indirectly reduce access to RBD epitopes^{99,100}. N331 is populated almost completely with complex glycans across all variants we studied (**Figure 3A**). N331 and N343 glycans are reported to shield the RBM in a “down” conformation⁴⁹. We observed that N343 is occupied almost completely with complex glycans in the Wuhan-Hu-1 strain, as well as in some of the variants, but a shift towards high mannose glycans was seen in Lambda, Beta, and this shift was statistically significant in Mu and Delta (for 6P versions) variants (**Figures 3A;4A,C**). These changes are highly relevant because glycans at N343 are implicated in pushing the RBD “up” into an “open” conformation⁴⁸, and is targeted by neutralizing antibodies^{90,92}.

S1-protein CTD

The NTD-associated subdomain-2 of S1-protein *i.e.*, CTD-1 and CTD-2 (**Figure 1B**) hosts 3 NGS (N603, N616 and N657). These 3 NGS, along with N61 and N801 in the S2-protein, are proximal to the proteolysis sites S1/S2 and S2'¹⁰¹. The glycans anchored to these NGS may affect access to Furin-like proteases through glycan holes around S1/S2, S2' and FP¹⁰². Though we abrogated the S1/S2 cleavage site in the spike-proteins used in this study, any fluctuation in glycosylation state at these NGS could provide evidence for an interaction of the S1/S2 region with glycans on N61/N603¹⁰³, and glycans on all 5 NGS that affect spike incorporation on virions and their capability to infect cells¹⁰¹. We observed a significantly higher proportion of high-mannose glycans on N603 and N801 in the 6P and 6P-Mut7 versus the 2P versions of Wuhan-Hu-1, as well as in all variants we studied except Gamma, where complex glycans are significantly higher at N603/N801 (**Figure 3A**). We find N61 and N657 to be almost completely occupied with complex glycans across all variants we studied (**Figure 3A**).

N616 is adjacent to D614G, which is conserved in all SARS-2 variants that have emerged since Wuhan-Hu-1. The D614G mutation is known to have significantly increased SARS-2 infectivity by reducing S1-shedding, thus ensuring that the spike is intact and available for receptor binding¹⁰⁴⁻¹⁰⁶. The stabilization of spike in D614G variants is attributed to the loss of an interaction between G614 in one protomer and a region immediately downstream of FP (amino acids 823-862) in a neighboring protomer, and the effect this plays on an adjacent loop (loop 630) that is proposed to play a critical role in modulating/regulating spike structure for viral fusion with host^{55,76,107,108}. Compared to Wuhan-Hu-1 where N616 is mostly occupied with complex glycans, Alpha, Beta, Delta, and Mu show significant shifts towards high-mannose glycans (**Figure 3A**). The absence of this shift maybe explained by the FP-proximal T859N mutation in Lambda and N856K mutation in Omicron, which could possibly counter the loss of inter-protomer interaction caused due to D614G¹⁰⁹⁻¹¹¹. The change in glycosylation state at N616 in variants can contribute to or be affected by the structural dynamics of D614G¹¹². This relationship has been postulated^{71,113}, but not systematically evaluated.

Discussion

The COVID-19 pandemic is driven by evolving variants of SARS-2, which are characterized by critical mutations that cause changes in the structure of the spike, hence affecting infectivity¹¹⁴. These structural modifications cause and are also affected by *N*-glycosylation changes. Using the 6P-Mut7 form of spike-protein from 7 SARS-2 variants, we present here a comprehensive analysis of changes in the site-specific *N*-glycan processing relative to Wuhan-Hu-1 (**Figure 3A,B,C**).

Using stabilized soluble spike-protein trimers hosting known variant-specific mutations, we observed that many NGS in NTD, RBD and stalk (N17/N20, N61, N74, N282, N331, N1158, N1173, N1194) exhibited near-complete occupancy with complex glycans, while N234 is occupied with high mannose glycans (**Figure 3A**). Glycosylation changes were limited to the NGS shown/predicted to be directly involved in: [1] RBD dynamics (N122, N149, N165 and N343) along with N234 (**Figure 3A**), [2] proteolysis/spike-stabilization by virtue of their proximity to S1/S2 and/or S2' (N603, N616, N657 and N801) along with N61 (**Figure 3A**), and [3] stabilization of post-fusion functions of S2-protein (N1074 and N1098) along with the 3 stalk NGS *i.e.*, N1158, N1173 and N1194 (**Figure 3A**). A recent analysis by Newby *et al.*⁹⁶ supports our observations, although their interpretations are based on only the 6P version while ours are based mostly on 6P-Mut7. Based only on 6P, Newby *et al.* observed very low glycan occupancy at N657, N1173 and N1194, which contrasts with what we observed (**Figure 4C**), though they previously reported almost complete occupancy with complex glycans at N1173 on Wuhan-Hu-1⁶⁵. Newby *et al.* also observed more high-mannose occupancy at N165 and N61 in Wuhan-Hu-1⁹⁶, which may have caused them to miss the glycosylation changes at N165 that we observe across variants (**Figure 3A**), and *vice-versa* for N61. Since we were unable to sample sufficient peptides for N709/N717 (these glycans possibly affect proteolysis/spike-stabilization) and N1134 (these glycans may play a role in post-fusion S2-protein stability) in many of the 6P/6P-Mut7 versions we analyzed, we refrained from commenting on their glycosylation state change, though Newby *et al.* found that the Beta, Gamma, Delta, Omicron and Wuhan-Hu-1 spikes are decorated with mostly high-mannose and complex glycans at N709/N717 and N1134, respectively⁹⁶. Using a hierarchical clustering analysis for similarity in glycosylation pattern among shared and "well-sampled" NGS in 6P-Mut7, we see that despite the huge number mutations in Omicron,

it is glycosylated more like Wuhan-Hu-1 than other variants, with Gamma and Delta being the most different (**Figure 3D**). This hierarchical cluster differs from the inferred evolutionary pattern of the SARS-2 variants determined by nucleic acid mutation analysis (**Figure 3E**, modified from <https://covariants.org/>), suggesting that selective pressure on glycan changes is more dependent on higher-order structure than primary sequence of a protein.

Unlike recent studies which used traditional glycoproteomic approaches to determine glycosylation state changes among a smaller set of SARS-2 variants^{96,115}, we used DeGlyPHER⁶³ for our analysis. DeGlyPHER provides the statistical power necessary to allow pairwise comparison of NGS to determine quantitative changes in unoccupied, high mannose and complex glycosylated states between variant spike-proteins. Traditional glycoproteomic/glycomic approaches can provide structural details of *N*-glycans and can discriminate between high-mannose and hybrid glycans, but they lack the statistical strength to determine site-specific glycosylation state changes between variants. DeGlyPHER's advantage is evident from the large number of statistically confident glycosylation state differences we identified, and their critical importance is validated by existing literature.

We observed many prominent shifts from complex glycans on Wuhan-Hu-1 to high mannose glycans on "variant" spikes, at multiple NGS (**Figure 3B**). This trend hints at reduced *N*-glycan processivity at these NGS, hence implying an increase in their steric occlusion. It also suggests that variant spikes may be better at using mannose-binding membrane proteins as receptors for host-cell entry/fusion¹¹⁶, thus explaining SARS-2 tropism in the lower human respiratory tract, where infection is most prominent but the primary host receptor (ACE2) is minimally expressed^{81,117}. This spike-glycan-based attachment of infectious virus to host cells can increase virus residence time on host surface, thus providing a better chance of host-virus fusion and consequent infection. Unlike the spike on an infectious virus, vaccine action is independent of cellular attachment or viral fusion, so the variant-based protein-structure changes are more likely to explain immunogenicity than the changes they effect in glycan landscapes. This notion was supported by studies that reported broader immunogenicity of partially-deglycosylated immunogens^{118,119}. We benchmarked the Novavax SARS-2 spike and found its glycan landscape to be very similar to the 2P version of the Wuhan-Hu-1 spike (**Figure 5A,B**), despite the absence of the TM and CT domains in the 2P version and both trimers being expressed in different cell types (2P version in human cells and Novavax vaccine in insect cells⁵⁵).

We observed the most conspicuous and consistent shifts from complex to high mannose glycans at N165, N343 and N616 (**Figure 3B**). Newby *et. al.* see similar increase in high-mannose (mostly M5) glycans at N165 and N616, and hybrid glycans at N616⁹⁶. Owing to structural changes in variant spike-proteins, Golgi α -mannosidase II (~130 kDa), that initiates processing of all complex glycans¹²⁰, may have limited access to process glycans at these NGS by virtue of its size, when compared to other mannosidases^{121,122} and glycosyl transferases^{123,124} (~40-70 kDa) that form M4-M6 high-mannose and hybrid glycans⁴⁶. N165 and N343 are implicated in RBD opening⁴⁸⁻⁵⁰, and N616 is a single amino acid away from D614G, which is the most consistent mutation in SARS-2 variants⁹ and implicated in critical structural changes that determine S1-S2 integrity after Furin cleavage^{107,125}. So, there is very high probability that N616 glycans can regulate the integrity of S1-S2 coupling in the spike-protein trimer⁷¹. Presence of *O*-glycans has been reported at N618, that may also contribute to this effect^{126,127}. P681R mutation may enhance Furin cleavage by adding a basic residue to 682RRAR in Delta and D614G stabilizes the Furin-cleaved S1-protein on S2-protein to facilitate fusogenicity, thus explaining Delta's high disease severity^{107,110,128,129}. The significant decrease in glycan processing at N616, N165 and N343 that we observed in Delta (**Figures 3A;4A,C**) may further explain fusogenicity and syncytia formation *via* mannose-binding receptors on respiratory tract cells that are the primary tissue affected by Delta but which sparsely express ACE2^{80,81,94,116,130,131}. Further interrogation of this possibility may bring a critical advance in understanding Delta's severe pathogenicity in human respiratory tissue.

Methods

Glycoprotein expression and Purification

Spike-proteins (amino acid sequences in **Supplementary Information**) were expressed and purified as previously described⁶⁷. Briefly, 500 µg of each plasmid encoding spike-proteins used in this study were incubated with 1.5 mg of polyethylenimine for 20 min and the mixture was deposited in 1L of HEK293F cells. Protein was expressed for 6 days, cells were harvested, and the protein was purified with a StrepTactin XT 4FLOW column. The eluted protein was then size exclusion purified over a Superose 6 HiLoad 16/600 pg 120 mL column.

Electron microscopy

To assess trimer homogeneity, 3 µL of spike-protein at 0.03 mg/ml in 1X TBS was deposited on a glow-discharged carbon coated copper mesh grid and blotted off. 3 µL of 2% uranyl formate was deposited on the grid for 90 s then blotted off. Data collection was done on a FEI Tecnai Spirit (120 keV) and a FEI Eagle 4k x 4k CCD camera and automated with the Leginon software¹³². Raw micrographs were stored in the Appion¹³³ database, and 2D classes were generated with RELION¹³⁴.

Mass spectrometry analysis

DeGlyPHER⁶³ was used to ascertain site-specific glycan occupancy and processivity on glycoproteins.

Proteinase K treatment and deglycosylation

Purified SARS-2 spike glycoproteins were exchanged to water using Microcon Ultracel PL-10 centrifugal filter. Glycoproteins were reduced with 5 mM tris(2-carboxyethyl)phosphine hydrochloride (TCEP-HCl) and alkylated with 10 mM 2-Chloroacetamide in 100 mM ammonium acetate for 20 min at room temperature (RT, 24°C). Initial protein-level deglycosylation was performed using 250 U of Endo H for 5 µg trimer, for 1 h at 37°C. Glycoproteins were digested with 1:25 Proteinase K (PK) for 30 min at 37°C (For NVX-CoV2373, 9 different conditions were used *viz.*, 16 h of trypsin digestion, and variations in PK treatment – 1:25 PK for 30 min, 1 h, 2 h, 4 h; 1:100, 1:500, 1:1000, 1:2000 PK for 4 h). PK was denatured by incubating at 90°C for 15 min, then cooled to RT. Peptides were deglycosylated again with 250 U Endo H for 1 h at 37°C, then frozen at –80°C and lyophilized. 100 U PNGase F was lyophilized, resuspended in 20 µl 100 mM ammonium bicarbonate prepared in H₂¹⁸O, and added to the lyophilized peptides. Reactions were then incubated for 1 h at 37°C, and subsequently analyzed by LC-MS/MS.

LC-MS/MS

Samples were analyzed on an Q Exactive HF-X mass spectrometer. Samples were injected directly onto a 25 cm, 100 µm ID column packed with BEH 1.7 µm C18 resin. Samples were separated at a flow rate of 300 nL/min on an EASY-nLC 1200 UHPLC. Buffers A and B were 0.1% formic acid in 5% and 80% acetonitrile, respectively. The following gradient was used: 1–25% B over 160 min, an increase to 40% B over 40 min, an increase to 90% B over another 10 min and 30 min at 90% B for a total run time of 240 min. Column was re-equilibrated with Buffer A prior to the injection of sample. Peptides were eluted from the tip of the column and nanosprayed directly into the mass spectrometer by application of 2.8 kV at the back of the column. The mass spectrometer was operated in a data dependent mode. Full MS1 scans were collected in the Orbitrap at 120,000 resolution. The ten most abundant ions per scan were selected for HCD MS/MS at 25 NCE. Dynamic exclusion was enabled with exclusion duration of 10 s and singly charged ions were excluded.

Data Processing

Protein and peptide identifications were made with Integrated Proteomics Pipeline (IP2). Tandem mass spectra were extracted from raw files using RawConverter¹³⁵ and searched with ProLuCID¹³⁶ against a database comprising UniProt reviewed (Swiss-Prot) proteome for Homo sapiens (UP000005640), UniProt amino acid sequences for Endo H (P04067), PNGase F (Q9XBM8), and Proteinase K (P06873), amino acid sequences for the examined proteins, and a list of general protein contaminants. The search space included no cleavage-specificity. Carbamidomethylation (+57.02146 C) was considered a static modification. Deamidation in presence of H₂¹⁸O (+2.988261 N), GlcNAc (+203.079373 N), oxidation

(+15.994915 M) and N-terminal pyroglutamate formation (−17.026549 Q) were considered differential modifications. Data was searched with 50 ppm precursor ion tolerance and 50 ppm fragment ion tolerance. Identified proteins were filtered using DTASelect2¹³⁷, utilizing a target-decoy database search strategy to limit the false discovery rate to 1%, at the spectrum level¹³⁸. A minimum of 1 peptide per protein and no tryptic end per peptide were required and precursor delta mass cut-off was fixed at 15 ppm. Statistical models for peptide mass modification (modstat) were applied. Censu2¹³⁹ label-free analysis was performed based on the precursor peak area, with a 15 ppm precursor mass tolerance and 0.1 min retention time tolerance. “Match between runs” was used to find missing peptides between runs. Data analysis using GlycoMSQuant⁶³ was implemented to automate the analysis. GlycoMSQuant summed precursor peak areas across replicates, discarded peptides without NGS, discarded misidentified peptides when N-glycan remnant-mass modifications were localized to non-NGS asparagines and corrected/fixed N-glycan mislocalization where appropriate. The results were aligned to NGS in spike of Wuhan-Hu-1 (UniProt #P0DTC2).

A glycosylated model⁴⁹ based on the “closed state” of SARS-2 spike-protein trimer (PDB: 6VXX)³⁸ and N-glycosylation profile determined by Watanabe *et. al.*⁵³ was uploaded on ChimeraX v.1.5 (<https://www.cgl.ucsf.edu/chimerax/>). Glycans were separated into separate PDB files using The PyMOL Molecular Graphics System v.2.5.2 (<https://pymol.org/>). Coordinates for membrane structure were hidden and glycans were color-coded using Python v.3.9.7 (<https://www.python.org/>) in multiple formats: [1] monochrome to highlight all glycans over protein sub-structure, [2] a 5-color gradient to classify the dominant proportion of unoccupied glycosylation sites, high-mannose/hybrid glycans and complex glycans, and [3] a 21-color gradient to represent percentage-point shift in proportion of high-mannose/hybrid glycans at a particular glycosylation site¹⁴⁰, when comparing 2 immunogens.

Proportional distribution of glycans at NGS common to all variants (*i.e.*, except N17, N20, N74 and N188, and the inconsistently sampled N709, N717 and N1134), as calculated by GlycoMSQuant⁶³, was condensed into a 1D feature vector, and a pairwise correlation analysis was conducted between all variants in their 6P-Mut7 versions. Subsequently, we used Scipy's hierarchical linkage function to cluster based on similarity and then used the hierarchical dendrogram function to visualize the results¹⁴¹.

Reagent or Resource	Source	Identifier
Chemicals/Consumables		
Microcon Ultracel PL-10 centrifugal filters	Millipore Sigma	Cat#MRCPRT010
Pierce TCEP HCl	Thermo Scientific	Cat#20490
Ammonium acetate ≥98%	Sigma-Aldrich	Cat#A1542
2-Chloroacetamide ≥98%	Sigma-Aldrich	Cat#22790
Endo H	New England Biolabs	Cat#P0702
Calcium chloride	Sigma-Aldrich	Cat#C5670
Proteinase K	Sigma-Aldrich	Cat#P2308
Trypsin	Promega	Cat#V5111
PNGase F	New England Biolabs	Cat#P0705
Ammonium bicarbonate ≥99.5%	Sigma Aldrich	CAT#09830
H ₂ ¹⁸ O (97% ¹⁸ O)	Sigma-Aldrich	Cat#329878
Resin, Acquity UPLC® BEH 1.7 μm C18	Waters	Cat#186004690
Water (Optima LC-MS grade)	Fisher Scientific	Cat#W6-4
Acetonitrile	Honeywell	Cat#AH015-4
Formic acid 90%	J.T.Baker	Cat#0129-01
Polymicro fused silica capillary tubing 100 μm	Molex	Cat#1068150023
11 PP Vial Crimp/Snap 250 μL	Thermo Scientific	Cat#C4011-13
Snap-it Seal	Thermo Scientific	Cat#C4011-53
0.2 mL Thin-walled Tubes	Thermo Scientific	Cat#AB-0620
Protein LoBind Tube 1.5 mL	Eppendorf	Cat#022431081
DeckWorks low binding pipette tips (200 μL)	Corning	Cat#4151
Pierce HeLa protein digest standard	Thermo Scientific	Cat#88329
Polyethylenimine HCl Max	Polysciences, Inc.	Cat# NC1038561

Copper mesh grid	Electron Microscopy Sciences	Cat#0400-Cu
Uranyl formate	Electron Microscopy Sciences	Cat#22451
NVX-CoV2373	Novavax, Inc.	https://www.novavax.com/science-technology/vaccine-pipeline/covid-19-vaccine
Deposited Data		
Mass spectrometry and proteomics analysis	Pride/MassIVE	Provided upon request
Graphics creation	GitHub	https://github.com/BhavyaSingh-Rolly/SARS-Visualization
Experimental Models: Cell lines		
HEK-293 Freestyle	Thermo Fisher	Cat#R79007
Software		
ProLuCID	IP2, Bruker Scientific LLC	http://fields.scripps.edu/yates/wp/?page_id=821
DTASelect2.0	IP2, Bruker Scientific LLC	http://fields.scripps.edu/yates/wp/?page_id=816
Census2.0	IP2, Bruker Scientific LLC	http://fields.scripps.edu/yates/wp/?page_id=824
GlycoMSQuant v.1.8.2	John R. Yates III, Scripps Research, La Jolla	https://github.com/proteomicsyates/GlycoMSQuant
RAWConverter	John R. Yates III, Scripps Research, La Jolla	http://fields.scripps.edu/rawconv/
Office 365	Microsoft	https://www.office.com/
XCalibur	Thermo Scientific	Cat#OPTON-30965-7
ChimeraX	UCSF	https://www.cgl.ucsf.edu/chimerax/
Leginon	Suloway <i>et al.</i> , 2005	https://emg.nysbc.org/edmine/projects/leginon/wiki/Leginon_Homepage
Appion	Lander <i>et al.</i> , 2009	N/A
RELION	Scheres <i>et al.</i> , 2012	https://relion.readthedocs.io/en/release-3.1/
SciPy	Virtanen <i>et al.</i> , 2020	https://scipy.org/
PyMOL v.2.5.2	Schrödinger, Inc.	https://pymol.org/
Python v.3.9.7	Python Software Foundation	https://www.python.org/
Instruments		
Q Exactive HF-X	Thermo Scientific	Cat#0726055
EASY-nLC 1200	Thermo Scientific	Cat#LC140
Laser-based micropipette puller system	Sutter Instrument	Cat#P-2000
Pressure bomb	customized with Swagelok	https://www.swagelok.com/
VirTis Freezemobile 25L Freeze Dryer	SP Scientific	Cat#100002172
MJ Mini Personal Thermal Cyclers	BioRad	Cat# PTC1148EDU
Microfuge18 centrifuge	Beckman Coulter	Cat#367160
AKTA Pure System	Cytiva	N/A

StrepTactin XT 4FLOW column	IBA Biosciences	Cat# NC1850510
Superose 6 HiLoad 16/600 pg 120 mL	Cytiva	Cat #29323952
Superose 6 Increase 10/300 GL	Cytiva	Cat#29091596
Tecnai Spirit Electron Microscope	FEI (Thermo Fisher)	N/A
Eagle 4k x4k CCD Camera	FEI (Thermo Fisher)	N/A

Contributions

S.B. conceptualized the project, performed glycan analysis, and wrote the manuscript with contribution of all authors. J.K.D. performed LC-MS/MS. J.L.T and J.C. produced the spike-proteins. J.L.T performed the NS-EM. B.S. created the molecular structure graphics. P.T.G. performed the hierarchical clustering analysis. J.C.P, A.B.W. and J.R.Y supervised the project.

Acknowledgements

We thank Claire Delahunty and Sandhya Bangaru for critically reading the manuscript, Charles Bowman for computational assistance, Salvador Martínez-Bartolomé for assistance with GlycoMSQuant, and Alessio D'Addabbo and Max Crispin (University of Southampton, UK) for pointing us to the use of percentage-point scale. We thank Nita Patel, Alyse D. Portnoff, and Gale E. Smith from Novavax, Inc. for supplying NVX-CoV2373 for this research. This work was supported by the grants P41GM103533 (NIH), UM1AI100663 (NIH, CHAVI-ID), UM1AI144462 (NIH, CHAVD), R01/R56AI113867 (NIH/NIAD) and Bill and Melinda Gates Foundation (INV-004923).

Competing Interests

The authors declare no competing financial interest.

References

1. Zhou, P., Yang, X.L., Wang, X.G., Hu, B., Zhang, L., Zhang, W., Si, H.R., Zhu, Y., Li, B., Huang, C.L., et al. (2020). A pneumonia outbreak associated with a new coronavirus of probable bat origin. *Nature* 579, 270-273. 10.1038/s41586-020-2012-7.
2. Wu, F., Zhao, S., Yu, B., Chen, Y.M., Wang, W., Song, Z.G., Hu, Y., Tao, Z.W., Tian, J.H., Pei, Y.Y., et al. (2020). A new coronavirus associated with human respiratory disease in China. *Nature* 579, 265-269. 10.1038/s41586-020-2008-3.
3. Cutler, D.M., and Summers, L.H. (2020). The COVID-19 Pandemic and the \$16 Trillion Virus. *Jama* 324, 1495-1496. 10.1001/jama.2020.19759.
4. Koelle, K., Martin, M.A., Antia, R., Lopman, B., and Dean, N.E. (2022). The changing epidemiology of SARS-CoV-2. *Science* 375, 1116-1121. 10.1126/science.abm4915.
5. Worobey, M., Levy, J.I., Malpica Serrano, L., Crits-Christoph, A., Pekar, J.E., Goldstein, S.A., Rasmussen, A.L., Kraemer, M.U.G., Newman, C., Koopmans, M.P.G., et al. (2022). The Huanan Seafood Wholesale Market in Wuhan was the early epicenter of the COVID-19 pandemic. *Science* 377, 951-959. 10.1126/science.abp8715.
6. Pekar, J.E., Magee, A., Parker, E., Moshiri, N., Izhikevich, K., Havens, J.L., Gangavarapu, K., Malpica Serrano, L.M., Crits-Christoph, A., Matteson, N.L., et al. (2022). The molecular epidemiology of multiple zoonotic origins of SARS-CoV-2. *Science* 377, 960-966. 10.1126/science.abp8337.
7. Gao, G., Liu, W., Liu, P., Lei, W., Jia, Z., He, X., Liu, L.-L., Shi, W., Tan, Y., Zou, S., et al. (2022). Surveillance of SARS-CoV-2 in the environment and animal samples of the Huanan Seafood Market. *Research Square*.
8. Tao, K., Tzou, P.L., Nouhin, J., Gupta, R.K., de Oliveira, T., Kosakovsky Pond, S.L., Fera, D., and Shafer, R.W. (2021). The biological and clinical significance of emerging SARS-CoV-2 variants. *Nat Rev Genet* 22, 757-773. 10.1038/s41576-021-00408-x.

9. Harvey, W.T., Carabelli, A.M., Jackson, B., Gupta, R.K., Thomson, E.C., Harrison, E.M., Ludden, C., Reeve, R., Rambaut, A., Peacock, S.J., and Robertson, D.L. (2021). SARS-CoV-2 variants, spike mutations and immune escape. *Nat Rev Microbiol* 19, 409-424. 10.1038/s41579-021-00573-0.
10. Tegally, H., Moir, M., Everatt, J., Giovanetti, M., Scheepers, C., Wilkinson, E., Subramoney, K., Makatini, Z., Moyo, S., Amoako, D.G., et al. (2022). Emergence of SARS-CoV-2 Omicron lineages BA.4 and BA.5 in South Africa. *Nat Med* 28, 1785-1790. 10.1038/s41591-022-01911-2.
11. Konings, F., Perkins, M.D., Kuhn, J.H., Pallen, M.J., Alm, E.J., Archer, B.N., Barakat, A., Bedford, T., Bhiman, J.N., Caly, L., et al. (2021). SARS-CoV-2 Variants of Interest and Concern naming scheme conducive for global discourse. *Nat Microbiol* 6, 821-823. 10.1038/s41564-021-00932-w.
12. Tang, J.W., Tambyah, P.A., and Hui, D.S. (2021). Emergence of a new SARS-CoV-2 variant in the UK. *J Infect* 82, e27-e28. 10.1016/j.jinf.2020.12.024.
13. Washington, N.L., Gangavarapu, K., Zeller, M., Bolze, A., Cirulli, E.T., Schiabor Barrett, K.M., Larsen, B.B., Anderson, C., White, S., Cassens, T., et al. (2021). Emergence and rapid transmission of SARS-CoV-2 B.1.1.7 in the United States. *Cell* 184, 2587-2594.e2587. 10.1016/j.cell.2021.03.052.
14. Tegally, H., Wilkinson, E., Giovanetti, M., Iranzadeh, A., Fonseca, V., Giandhari, J., Doolabh, D., Pillay, S., San, E.J., Msomi, N., et al. (2021). Detection of a SARS-CoV-2 variant of concern in South Africa. *Nature* 592, 438-443. 10.1038/s41586-021-03402-9.
15. Faria, N.R., Mellan, T.A., Whittaker, C., Claro, I.M., Candido, D.D.S., Mishra, S., Crispim, M.A.E., Sales, F.C.S., Hawryluk, I., McCrone, J.T., et al. (2021). Genomics and epidemiology of the P.1 SARS-CoV-2 lineage in Manaus, Brazil. *Science* 372, 815-821. 10.1126/science.abh2644.
16. Mlcochova, P., Kemp, S.A., Dhar, M.S., Papa, G., Meng, B., Ferreira, I., Datir, R., Collier, D.A., Albecka, A., Singh, S., et al. (2021). SARS-CoV-2 B.1.617.2 Delta variant replication and immune evasion. *Nature* 599, 114-119. 10.1038/s41586-021-03944-y.
17. Viana, R., Moyo, S., Amoako, D.G., Tegally, H., Scheepers, C., Althaus, C.L., Anyaneji, U.J., Bester, P.A., Boni, M.F., Chand, M., et al. (2022). Rapid epidemic expansion of the SARS-CoV-2 Omicron variant in southern Africa. *Nature* 603, 679-686. 10.1038/s41586-022-04411-y.
18. Laiton-Donato, K., Franco-Muñoz, C., Álvarez-Díaz, D.A., Ruiz-Moreno, H.A., Usme-Ciro, J.A., Prada, D.A., Reales-González, J., Corchuelo, S., Herrera-Sepúlveda, M.T., Naizaque, J., et al. (2021). Characterization of the emerging B.1.621 variant of interest of SARS-CoV-2. *Infect Genet Evol* 95, 105038. 10.1016/j.meegid.2021.105038.
19. Halfmann, P.J., Kuroda, M., Armbrust, T., Theiler, J., Balaram, A., Moreno, G.K., Accola, M.A., Iwatsuki-Horimoto, K., Valdez, R., Stoneman, E., et al. (2022). Characterization of the SARS-CoV-2 B.1.621 (Mu) variant. *Sci Transl Med* 14, eabm4908. 10.1126/scitranslmed.abm4908.
20. Romero, P.E., Dávila-Barclay, A., Salvatierra, G., González, L., Cuicapuza, D., Solís, L., Marcos-Carbajal, P., Huancachoque, J., Maturrano, L., and Tsukayama, P. (2021). The Emergence of Sars-CoV-2 Variant Lambda (C.37) in South America. *Microbiol Spectr* 9, e0078921. 10.1128/Spectrum.00789-21.
21. Haynes, B.F., Wiehe, K., Borror, P., Saunders, K.O., Korber, B., Wagh, K., McMichael, A.J., Kelsoe, G., Hahn, B.H., Alt, F., and Shaw, G.M. (2022). Strategies for HIV-1 vaccines that induce broadly neutralizing antibodies. *Nat Rev Immunol*, 1-17. 10.1038/s41577-022-00753-w.
22. Burton, D.R., and Hangartner, L. (2016). Broadly Neutralizing Antibodies to HIV and Their Role in Vaccine Design. *Annu Rev Immunol* 34, 635-659. 10.1146/annurev-immunol-041015-055515.
23. Leggat, D.J., Cohen, K.W., Willis, J.R., Fulp, W.J., deCamp, A.C., Kalyuzhniy, O., Cottrell, C.A., Menis, S., Finak, G., Ballweber-Fleming, L., et al. (2022). Vaccination induces HIV broadly neutralizing antibody precursors in humans. *Science* 378, eadd6502. 10.1126/science.add6502.
24. Wilson, I.A., Skehel, J.J., and Wiley, D.C. (1981). Structure of the haemagglutinin membrane glycoprotein of influenza virus at 3 Å resolution. *Nature* 289, 366-373. 10.1038/289366a0.
25. Kirchdoerfer, R.N., Cottrell, C.A., Wang, N., Pallesen, J., Yassine, H.M., Turner, H.L., Corbett, K.S., Graham, B.S., McLellan, J.S., and Ward, A.B. (2016). Pre-fusion structure of a human coronavirus spike protein. *Nature* 531, 118-121. 10.1038/nature17200.
26. Pallesen, J., Wang, N., Corbett, K.S., Wrapp, D., Kirchdoerfer, R.N., Turner, H.L., Cottrell, C.A., Becker, M.M., Wang, L., Shi, W., et al. (2017). Immunogenicity and structures of a rationally designed prefusion MERS-CoV spike antigen. *Proc Natl Acad Sci U S A* 114, E7348-e7357. 10.1073/pnas.1707304114.
27. Lyumkis, D., Julien, J.P., de Val, N., Cupo, A., Potter, C.S., Klasse, P.J., Burton, D.R., Sanders, R.W., Moore, J.P., Carragher, B., et al. (2013). Cryo-EM structure of a fully glycosylated soluble cleaved HIV-1 envelope trimer. *Science* 342, 1484-1490. 10.1126/science.1245627.

28. Julien, J.P., Cupo, A., Sok, D., Stanfield, R.L., Lyumkis, D., Deller, M.C., Klasse, P.J., Burton, D.R., Sanders, R.W., Moore, J.P., et al. (2013). Crystal structure of a soluble cleaved HIV-1 envelope trimer. *Science* 342, 1477-1483. 10.1126/science.1245625.
29. Kanekiyo, M., and Graham, B.S. (2021). Next-Generation Influenza Vaccines. *Cold Spring Harb Perspect Med* 11. 10.1101/cshperspect.a038448.
30. Wrapp, D., Wang, N., Corbett, K.S., Goldsmith, J.A., Hsieh, C.L., Abiona, O., Graham, B.S., and McLellan, J.S. (2020). Cryo-EM structure of the 2019-nCoV spike in the prefusion conformation. *Science* 367, 1260-1263. 10.1126/science.abb2507.
31. Mulligan, M.J., Lyke, K.E., Kitchin, N., Absalon, J., Gurtman, A., Lockhart, S., Neuzil, K., Raabe, V., Bailey, R., Swanson, K.A., et al. (2020). Phase I/II study of COVID-19 RNA vaccine BNT162b1 in adults. *Nature* 586, 589-593. 10.1038/s41586-020-2639-4.
32. Jackson, L.A., Anderson, E.J., Roupael, N.G., Roberts, P.C., Makhene, M., Coler, R.N., McCullough, M.P., Chappell, J.D., Denison, M.R., Stevens, L.J., et al. (2020). An mRNA Vaccine against SARS-CoV-2 - Preliminary Report. *N Engl J Med* 383, 1920-1931. 10.1056/NEJMoa2022483.
33. Sadoff, J., Le Gars, M., Shukarev, G., Heerwegh, D., Truyers, C., de Groot, A.M., Stoop, J., Tete, S., Van Damme, W., Leroux-Roels, I., et al. (2021). Interim Results of a Phase 1-2a Trial of Ad26.COV2.S Covid-19 Vaccine. *N Engl J Med* 384, 1824-1835. 10.1056/NEJMoa2034201.
34. Voysey, M., Clemens, S.A.C., Madhi, S.A., Weckx, L.Y., Folegatti, P.M., Aley, P.K., Angus, B., Baillie, V.L., Barnabas, S.L., Borat, Q.E., et al. (2021). Safety and efficacy of the ChAdOx1 nCoV-19 vaccine (AZD1222) against SARS-CoV-2: an interim analysis of four randomised controlled trials in Brazil, South Africa, and the UK. *Lancet* 397, 99-111. 10.1016/s0140-6736(20)32661-1.
35. Ella, R., Reddy, S., Blackwelder, W., Potdar, V., Yadav, P., Sarangi, V., Aileni, V.K., Kanungo, S., Rai, S., Reddy, P., et al. (2021). Efficacy, safety, and lot-to-lot immunogenicity of an inactivated SARS-CoV-2 vaccine (BBV152): interim results of a randomised, double-blind, controlled, phase 3 trial. *Lancet* 398, 2173-2184. 10.1016/s0140-6736(21)02000-6.
36. Logunov, D.Y., Dolzhikova, I.V., Shcheblyakov, D.V., Tukhvatulin, A.I., Zubkova, O.V., Dzharullaeva, A.S., Kovyrshina, A.V., Lubenets, N.L., Grousova, D.M., Erokhova, A.S., et al. (2021). Safety and efficacy of an rAd26 and rAd5 vector-based heterologous prime-boost COVID-19 vaccine: an interim analysis of a randomised controlled phase 3 trial in Russia. *Lancet* 397, 671-681. 10.1016/s0140-6736(21)00234-8.
37. Heinz, F.X., and Stiasny, K. (2021). Distinguishing features of current COVID-19 vaccines: knowns and unknowns of antigen presentation and modes of action. *NPJ Vaccines* 6, 104. 10.1038/s41541-021-00369-6.
38. Walls, A.C., Park, Y.J., Tortorici, M.A., Wall, A., McGuire, A.T., and Velesler, D. (2020). Structure, Function, and Antigenicity of the SARS-CoV-2 Spike Glycoprotein. *Cell* 181, 281-292.e286. 10.1016/j.cell.2020.02.058.
39. Lan, J., Ge, J., Yu, J., Shan, S., Zhou, H., Fan, S., Zhang, Q., Shi, X., Wang, Q., Zhang, L., and Wang, X. (2020). Structure of the SARS-CoV-2 spike receptor-binding domain bound to the ACE2 receptor. *Nature* 581, 215-220. 10.1038/s41586-020-2180-5.
40. Wolf, K.A., Kwan, J.C., and Kamil, J.P. (2022). Structural Dynamics and Molecular Evolution of the SARS-CoV-2 Spike Protein. *mBio* 13, e0203021. 10.1128/mbio.02030-21.
41. V'Kovski, P., Kratzel, A., Steiner, S., Stalder, H., and Thiel, V. (2021). Coronavirus biology and replication: implications for SARS-CoV-2. *Nat Rev Microbiol* 19, 155-170. 10.1038/s41579-020-00468-6.
42. Jackson, C.B., Farzan, M., Chen, B., and Choe, H. (2022). Mechanisms of SARS-CoV-2 entry into cells. *Nat Rev Mol Cell Biol* 23, 3-20. 10.1038/s41580-021-00418-x.
43. Marshall, R.D. (1972). Glycoproteins. *Annu Rev Biochem* 41, 673-702. 10.1146/annurev.bi.41.070172.003325.
44. Schjoldager, K.T., Narimatsu, Y., Joshi, H.J., and Clausen, H. (2020). Global view of human protein glycosylation pathways and functions. *Nat Rev Mol Cell Biol* 21, 729-749. 10.1038/s41580-020-00294-x.
45. Cao, L., Diedrich, J.K., Ma, Y., Wang, N., Pauthner, M., Park, S.R., Delahunty, C.M., McLellan, J.S., Burton, D.R., Yates, J.R., and Paulson, J.C. (2018). Global site-specific analysis of glycoprotein N-glycan processing. *Nat Protoc* 13, 1196-1212. 10.1038/nprot.2018.024.
46. Watanabe, Y., Bowden, T.A., Wilson, I.A., and Crispin, M. (2019). Exploitation of glycosylation in enveloped virus pathobiology. *Biochim Biophys Acta Gen Subj* 1863, 1480-1497. 10.1016/j.bbagen.2019.05.012.
47. Chawla, H., Fadda, E., and Crispin, M. (2022). Principles of SARS-CoV-2 glycosylation. *Curr Opin Struct Biol* 75, 102402. 10.1016/j.sbi.2022.102402.

48. Sztain, T., Ahn, S.H., Bogetti, A.T., Casalino, L., Goldsmith, J.A., Seitz, E., McCool, R.S., Kearns, F.L., Acosta-Reyes, F., Maji, S., et al. (2021). A glycan gate controls opening of the SARS-CoV-2 spike protein. *Nat Chem* 13, 963-968. 10.1038/s41557-021-00758-3.
49. Casalino, L., Gaieb, Z., Goldsmith, J.A., Hjorth, C.K., Dommer, A.C., Harbison, A.M., Fogarty, C.A., Barros, E.P., Taylor, B.C., McLellan, J.S., et al. (2020). Beyond Shielding: The Roles of Glycans in the SARS-CoV-2 Spike Protein. *ACS Cent Sci* 6, 1722-1734. 10.1021/acscentsci.0c01056.
50. Pang, Y.T., Acharya, A., Lynch, D.L., Pavlova, A., and Gumbart, J.C. (2022). SARS-CoV-2 spike opening dynamics and energetics reveal the individual roles of glycans and their collective impact. *Commun Biol* 5, 1170. 10.1038/s42003-022-04138-6.
51. Thompson, A.J., de Vries, R.P., and Paulson, J.C. (2019). Virus recognition of glycan receptors. *Curr Opin Virol* 34, 117-129. 10.1016/j.coviro.2019.01.004.
52. Watanabe, Y., Berndsen, Z.T., Raghvani, J., Seabright, G.E., Allen, J.D., Pybus, O.G., McLellan, J.S., Wilson, I.A., Bowden, T.A., Ward, A.B., and Crispin, M. (2020). Vulnerabilities in coronavirus glycan shields despite extensive glycosylation. *Nat Commun* 11, 2688. 10.1038/s41467-020-16567-0.
53. Watanabe, Y., Allen, J.D., Wrapp, D., McLellan, J.S., and Crispin, M. (2020). Site-specific glycan analysis of the SARS-CoV-2 spike. *Science* 369, 330-333. 10.1126/science.abb9983.
54. Zhang, S., Go, E.P., Ding, H., Anang, S., Kappes, J.C., Desaire, H., and Sodroski, J.G. (2022). Analysis of Glycosylation and Disulfide Bonding of Wild-Type SARS-CoV-2 Spike Glycoprotein. *J Virol* 96, e0162621. 10.1128/jvi.01626-21.
55. Bangaru, S., Ozorowski, G., Turner, H.L., Antanasijevic, A., Huang, D., Wang, X., Torres, J.L., Diedrich, J.K., Tian, J.H., Portnoff, A.D., et al. (2020). Structural analysis of full-length SARS-CoV-2 spike protein from an advanced vaccine candidate. *Science* 370, 1089-1094. 10.1126/science.abe1502.
56. Allen, J.D., Chawla, H., Samsudin, F., Zuzic, L., Shivgan, A.T., Watanabe, Y., He, W.T., Callaghan, S., Song, G., Yong, P., et al. (2021). Site-Specific Steric Control of SARS-CoV-2 Spike Glycosylation. *Biochemistry* 60, 2153-2169. 10.1021/acs.biochem.1c00279.
57. Zhao, P., Praissman, J.L., Grant, O.C., Cai, Y., Xiao, T., Rosenbalm, K.E., Aoki, K., Kellman, B.P., Bridger, R., Barouch, D.H., et al. (2020). Virus-Receptor Interactions of Glycosylated SARS-CoV-2 Spike and Human ACE2 Receptor. *Cell Host Microbe* 28, 586-601.e586. 10.1016/j.chom.2020.08.004.
58. Gobeil, S.M., Janowska, K., McDowell, S., Mansouri, K., Parks, R., Stalls, V., Kopp, M.F., Manne, K., Li, D., Wiehe, K., et al. (2021). Effect of natural mutations of SARS-CoV-2 on spike structure, conformation, and antigenicity. *Science* 373. 10.1126/science.abi6226.
59. Yuan, M., Huang, D., Lee, C.D., Wu, N.C., Jackson, A.M., Zhu, X., Liu, H., Peng, L., van Gils, M.J., Sanders, R.W., et al. (2021). Structural and functional ramifications of antigenic drift in recent SARS-CoV-2 variants. *Science* 373, 818-823. 10.1126/science.abh1139.
60. Zhang, J., Xiao, T., Cai, Y., and Chen, B. (2021). Structure of SARS-CoV-2 spike protein. *Curr Opin Virol* 50, 173-182. 10.1016/j.coviro.2021.08.010.
61. Wang, Z., Muecksch, F., Cho, A., Gaebler, C., Hoffmann, H.-H., Ramos, V., Zong, S., Cipolla, M., Johnson, B., Schmidt, F., et al. (2022). Conserved Neutralizing Epitopes on the N-Terminal Domain of Variant SARS-CoV-2 Spike Proteins. *bioRxiv*, 2022.2002.2001.478695. 10.1101/2022.02.01.478695.
62. Cerutti, G., Guo, Y., Zhou, T., Gorman, J., Lee, M., Rapp, M., Reddem, E.R., Yu, J., Bahna, F., Bimela, J., et al. (2021). Potent SARS-CoV-2 neutralizing antibodies directed against spike N-terminal domain target a single supersite. *Cell Host Microbe* 29, 819-833.e817. 10.1016/j.chom.2021.03.005.
63. Baboo, S., Diedrich, J.K., Martínez-Bartolomé, S., Wang, X., Schiffner, T., Groschel, B., Schief, W.R., Paulson, J.C., and Yates, J.R., 3rd (2021). DeGLYPHER: An Ultrasensitive Method for the Analysis of Viral Spike N-Glycoforms. *Anal Chem* 93, 13651-13657. 10.1021/acs.analchem.1c03059.
64. Baboo, S., Diedrich, J.K., Martínez-Bartolomé, S., Wang, X., Schiffner, T., Groschel, B., Schief, W.R., Paulson, J.C., and Yates, J.R. (2022). DeGLYPHER: Highly sensitive site-specific analysis of N-linked glycans on proteins. In *Methods in Enzymology*, (Academic Press). <https://doi.org/10.1016/bs.mie.2022.09.004>.
65. Chawla, H., Jossi, S.E., Faustini, S.E., Samsudin, F., Allen, J.D., Watanabe, Y., Newby, M.L., Marcial-Juárez, E., Lamerton, R.E., McLellan, J.S., et al. (2022). Glycosylation and Serological Reactivity of an Expression-enhanced SARS-CoV-2 Viral Spike Mimetic. *J Mol Biol* 434, 167332. 10.1016/j.jmb.2021.167332.
66. Hsieh, C.L., Goldsmith, J.A., Schaub, J.M., DiVenere, A.M., Kuo, H.C., Javanmardi, K., Le, K.C., Wrapp, D., Lee, A.G., Liu, Y., et al. (2020). Structure-based design of prefusion-stabilized SARS-CoV-2 spikes. *Science* 369, 1501-1505. 10.1126/science.abd0826.

67. Torres, J.L., Ozorowski, G., Andreano, E., Liu, H., Copps, J., Piccini, G., Donnici, L., Conti, M., Planchais, C., Planas, D., et al. (2022). Structural insights of a highly potent pan-neutralizing SARS-CoV-2 human monoclonal antibody. *Proc Natl Acad Sci U S A* *119*, e2120976119. [10.1073/pnas.2120976119](https://doi.org/10.1073/pnas.2120976119).
68. Allen, J.D., Ivory, D.P., Song, S.G., He, W.T., Capozzola, T., Yong, P., Burton, D.R., Andrabi, R., and Crispin, M. (2023). The diversity of the glycan shield of sarbecoviruses related to SARS-CoV-2. *Cell Rep* *42*, 112307. [10.1016/j.celrep.2023.112307](https://doi.org/10.1016/j.celrep.2023.112307).
69. Zhou, P., Yuan, M., Song, G., Beutler, N., Shaabani, N., Huang, D., He, W.T., Zhu, X., Callaghan, S., Yong, P., et al. (2022). A human antibody reveals a conserved site on beta-coronavirus spike proteins and confers protection against SARS-CoV-2 infection. *Sci Transl Med* *14*, eabi9215. [10.1126/scitranslmed.abi9215](https://doi.org/10.1126/scitranslmed.abi9215).
70. Turoňová, B., Sikora, M., Schürmann, C., Hagen, W.J.H., Welsch, S., Blanc, F.E.C., von Bülow, S., Gecht, M., Bagola, K., Hörner, C., et al. (2020). In situ structural analysis of SARS-CoV-2 spike reveals flexibility mediated by three hinges. *Science* *370*, 203-208. [10.1126/science.abd5223](https://doi.org/10.1126/science.abd5223).
71. Korber, B., Fischer, W.M., Gnanakaran, S., Yoon, H., Theiler, J., Abfalterer, W., Hengartner, N., Giorgi, E.E., Bhattacharya, T., Foley, B., et al. (2020). Tracking Changes in SARS-CoV-2 Spike: Evidence that D614G Increases Infectivity of the COVID-19 Virus. *Cell* *182*, 812-827.e819. [10.1016/j.cell.2020.06.043](https://doi.org/10.1016/j.cell.2020.06.043).
72. Martin, D.P., Weaver, S., Tegally, H., San, J.E., Shank, S.D., Wilkinson, E., Lucaci, A.G., Giandhari, J., Naidoo, S., Pillay, Y., et al. (2021). The emergence and ongoing convergent evolution of the SARS-CoV-2 N501Y lineages. *Cell* *184*, 5189-5200.e5187. [10.1016/j.cell.2021.09.003](https://doi.org/10.1016/j.cell.2021.09.003).
73. Liu, Y., Liu, J., Plante, K.S., Plante, J.A., Xie, X., Zhang, X., Ku, Z., An, Z., Scharton, D., Schindewolf, C., et al. (2022). The N501Y spike substitution enhances SARS-CoV-2 infection and transmission. *Nature* *602*, 294-299. [10.1038/s41586-021-04245-0](https://doi.org/10.1038/s41586-021-04245-0).
74. Alkhatib, M., Svicher, V., Salpini, R., Ambrosio, F.A., Bellocchi, M.C., Carioti, L., Piermatteo, L., Scutari, R., Costa, G., Artese, A., et al. (2021). SARS-CoV-2 Variants and Their Relevant Mutational Profiles: Update Summer 2021. *Microbiol Spectr* *9*, e0109621. [10.1128/Spectrum.01096-21](https://doi.org/10.1128/Spectrum.01096-21).
75. Iketani, S., Liu, L., Guo, Y., Liu, L., Chan, J.F., Huang, Y., Wang, M., Luo, Y., Yu, J., Chu, H., et al. (2022). Antibody evasion properties of SARS-CoV-2 Omicron sublineages. *Nature* *604*, 553-556. [10.1038/s41586-022-04594-4](https://doi.org/10.1038/s41586-022-04594-4).
76. Cai, Y., Zhang, J., Xiao, T., Peng, H., Sterling, S.M., Walsh, R.M., Jr., Rawson, S., Rits-Volloch, S., and Chen, B. (2020). Distinct conformational states of SARS-CoV-2 spike protein. *Science* *369*, 1586-1592. [10.1126/science.abd4251](https://doi.org/10.1126/science.abd4251).
77. Yao, H., Song, Y., Chen, Y., Wu, N., Xu, J., Sun, C., Zhang, J., Weng, T., Zhang, Z., Wu, Z., et al. (2020). Molecular Architecture of the SARS-CoV-2 Virus. *Cell* *183*, 730-738.e713. [10.1016/j.cell.2020.09.018](https://doi.org/10.1016/j.cell.2020.09.018).
78. Fan, X., Cao, D., Kong, L., and Zhang, X. (2020). Cryo-EM analysis of the post-fusion structure of the SARS-CoV spike glycoprotein. *Nat Commun* *11*, 3618. [10.1038/s41467-020-17371-6](https://doi.org/10.1038/s41467-020-17371-6).
79. Dodero-Rojas, E., Onuchic, J.N., and Whitford, P.C. (2021). Sterically confined rearrangements of SARS-CoV-2 Spike protein control cell invasion. *Elife* *10*. [10.7554/eLife.70362](https://doi.org/10.7554/eLife.70362).
80. Guo, L., Liang, Y., Li, H., Zheng, H., Yang, Z., Chen, Y., Zhao, X., Li, J., Li, B., Shi, H., et al. (2021). Epigenetic glycosylation of SARS-CoV-2 impact viral infection through DC&L-SIGN receptors. *iScience* *24*, 103426. [10.1016/j.isci.2021.103426](https://doi.org/10.1016/j.isci.2021.103426).
81. Zhang, J., Xiao, T., Cai, Y., Lavine, C.L., Peng, H., Zhu, H., Anand, K., Tong, P., Gautam, A., Mayer, M.L., et al. (2021). Membrane fusion and immune evasion by the spike protein of SARS-CoV-2 Delta variant. *Science* *374*, 1353-1360. [10.1126/science.abl9463](https://doi.org/10.1126/science.abl9463).
82. Chi, X., Yan, R., Zhang, J., Zhang, G., Zhang, Y., Hao, M., Zhang, Z., Fan, P., Dong, Y., Yang, Y., et al. (2020). A neutralizing human antibody binds to the N-terminal domain of the Spike protein of SARS-CoV-2. *Science* *369*, 650-655. [10.1126/science.abc6952](https://doi.org/10.1126/science.abc6952).
83. Yang, T.-J., Yu, P.-Y., Chang, Y.-C., Chang, N.-E., Tsai, Y.-X., Liang, K.-H., Draczkowski, P., Lin, B., Wang, Y.-S., Chien, Y.-C., et al. (2021). Structure-activity relationships of B.1.617 and other SARS-CoV-2 spike variants. *bioRxiv*, 2021.2009.2012.459978. [10.1101/2021.09.12.459978](https://doi.org/10.1101/2021.09.12.459978).
84. McCallum, M., De Marco, A., Lempp, F.A., Tortorici, M.A., Pinto, D., Walls, A.C., Beltramello, M., Chen, A., Liu, Z., Zatta, F., et al. (2021). N-terminal domain antigenic mapping reveals a site of vulnerability for SARS-CoV-2. *Cell* *184*, 2332-2347.e2316. [10.1016/j.cell.2021.03.028](https://doi.org/10.1016/j.cell.2021.03.028).
85. McCallum, M., Walls, A.C., Sprouse, K.R., Bowen, J.E., Rosen, L.E., Dang, H.V., De Marco, A., Franko, N., Tilles, S.W., Logue, J., et al. (2021). Molecular basis of immune evasion by the Delta and Kappa SARS-CoV-2 variants. *Science* *374*, 1621-1626. [10.1126/science.abl8506](https://doi.org/10.1126/science.abl8506).

86. Kimura, I., Kosugi, Y., Wu, J., Zahradnik, J., Yamasoba, D., Butlertanaka, E.P., Tanaka, Y.L., Uriu, K., Liu, Y., Morizako, N., et al. (2022). The SARS-CoV-2 Lambda variant exhibits enhanced infectivity and immune resistance. *Cell Rep* 38, 110218. [10.1016/j.celrep.2021.110218](https://doi.org/10.1016/j.celrep.2021.110218).
87. Pascarella, S., Ciccozzi, M., Bianchi, M., Benvenuto, D., Giovanetti, M., Cauda, R., and Cassone, A. (2021). Shortening Epitopes to Survive: The Case of SARS-CoV-2 Lambda Variant. *Biomolecules* 11. [10.3390/biom11101494](https://doi.org/10.3390/biom11101494).
88. Liu, H., Wei, P., Zhang, Q., Aviszus, K., Linderberger, J., Yang, J., Liu, J., Chen, Z., Waheed, H., Reynoso, L., et al. (2021). The Lambda variant of SARS-CoV-2 has a better chance than the Delta variant to escape vaccines. *bioRxiv*. [10.1101/2021.08.25.457692](https://doi.org/10.1101/2021.08.25.457692).
89. Choi, Y.K., Cao, Y., Frank, M., Woo, H., Park, S.J., Yeom, M.S., Croll, T.I., Seok, C., and Im, W. (2021). Structure, Dynamics, Receptor Binding, and Antibody Binding of the Fully Glycosylated Full-Length SARS-CoV-2 Spike Protein in a Viral Membrane. *J Chem Theory Comput* 17, 2479-2487. [10.1021/acs.jctc.0c01144](https://doi.org/10.1021/acs.jctc.0c01144).
90. Pinto, D., Park, Y.J., Beltramello, M., Walls, A.C., Tortorici, M.A., Bianchi, S., Jaconi, S., Culap, K., Zatta, F., De Marco, A., et al. (2020). Cross-neutralization of SARS-CoV-2 by a human monoclonal SARS-CoV antibody. *Nature* 583, 290-295. [10.1038/s41586-020-2349-y](https://doi.org/10.1038/s41586-020-2349-y).
91. Chen, R.E., Winkler, E.S., Case, J.B., Aziati, I.D., Bricker, T.L., Joshi, A., Darling, T.L., Ying, B., Errico, J.M., Shrihari, S., et al. (2021). In vivo monoclonal antibody efficacy against SARS-CoV-2 variant strains. *Nature* 596, 103-108. [10.1038/s41586-021-03720-y](https://doi.org/10.1038/s41586-021-03720-y).
92. Fang, Y., Sun, P., Xie, X., Du, M., Du, F., Ye, J., Kalveram, B.K., Plante, J.A., Plante, K.S., Li, B., et al. (2022). An antibody that neutralizes SARS-CoV-1 and SARS-CoV-2 by binding to a conserved spike epitope outside the receptor binding motif. *Sci Immunol*, eabp9962. [10.1126/sciimmunol.abp9962](https://doi.org/10.1126/sciimmunol.abp9962).
93. Lempp, F.A., Soriaga, L.B., Montiel-Ruiz, M., Benigni, F., Noack, J., Park, Y.J., Bianchi, S., Walls, A.C., Bowen, J.E., Zhou, J., et al. (2021). Lectins enhance SARS-CoV-2 infection and influence neutralizing antibodies. *Nature* 598, 342-347. [10.1038/s41586-021-03925-1](https://doi.org/10.1038/s41586-021-03925-1).
94. Soh, W.T., Liu, Y., Nakayama, E.E., Ono, C., Torii, S., Nakagami, H., Matsuura, Y., Shioda, T., and Arase, H. (2020). The N-terminal domain of spike glycoprotein mediates SARS-CoV-2 infection by associating with L-SIGN and DC-SIGN. *bioRxiv*, 2020.2011.2005.369264. [10.1101/2020.11.05.369264](https://doi.org/10.1101/2020.11.05.369264).
95. Henderson, R., Edwards, R.J., Mansouri, K., Janowska, K., Stalls, V., Kopp, M., Haynes, B.F., and Acharya, P. (2020). Glycans on the SARS-CoV-2 Spike Control the Receptor Binding Domain Conformation. *bioRxiv*. [10.1101/2020.06.26.173765](https://doi.org/10.1101/2020.06.26.173765).
96. Newby, M.L., Fogarty, C.A., Allen, J.D., Butler, J., Fadda, E., and Crispin, M. (2022). Variations within the glycan shield of SARS-CoV-2 impact viral spike dynamics. *J Mol Biol*, 167928. [10.1016/j.jmb.2022.167928](https://doi.org/10.1016/j.jmb.2022.167928).
97. Wang, Q., Iketani, S., Li, Z., Liu, L., Guo, Y., Huang, Y., Bowen, A.D., Liu, M., Wang, M., Yu, J., et al. (2023). Alarming antibody evasion properties of rising SARS-CoV-2 BQ and XBB subvariants. *Cell* 186, 279-286.e278. [10.1016/j.cell.2022.12.018](https://doi.org/10.1016/j.cell.2022.12.018).
98. Fallon, L., Belfon, K.A.A., Raguette, L., Wang, Y., Stepanenko, D., Cuomo, A., Guerra, J., Budhan, S., Varghese, S., Corbo, C.P., et al. (2021). Free Energy Landscapes from SARS-CoV-2 Spike Glycoprotein Simulations Suggest that RBD Opening Can Be Modulated via Interactions in an Allosteric Pocket. *J Am Chem Soc* 143, 11349-11360. [10.1021/jacs.1c00556](https://doi.org/10.1021/jacs.1c00556).
99. Liu, L., Casner, R.G., Guo, Y., Wang, Q., Iketani, S., Chan, J.F., Yu, J., Dadonaite, B., Nair, M.S., Mohri, H., et al. (2023). Antibodies that neutralize all current SARS-CoV-2 variants of concern by conformational locking. *bioRxiv*. [10.1101/2023.04.08.536123](https://doi.org/10.1101/2023.04.08.536123).
100. Seow, J., Khan, H., Rosa, A., Calvaresi, V., Graham, C., Pickering, S., Pye, V.E., Cronin, N.B., Huettner, I., Malim, M.H., et al. (2022). A neutralizing epitope on the SD1 domain of SARS-CoV-2 spike targeted following infection and vaccination. *Cell Rep* 40, 111276. [10.1016/j.celrep.2022.111276](https://doi.org/10.1016/j.celrep.2022.111276).
101. Yang, Q., Kelkar, A., Sriram, A., Hombu, R., Hughes, T.A., and Neelamegham, S. (2022). Role for N-glycans and calnexin-calreticulin chaperones in SARS-CoV-2 Spike maturation and viral infectivity. *Sci Adv* 8, eabq8678. [10.1126/sciadv.abq8678](https://doi.org/10.1126/sciadv.abq8678).
102. Xu, C., Wang, Y., Liu, C., Zhang, C., Han, W., Hong, X., Wang, Y., Hong, Q., Wang, S., Zhao, Q., et al. (2021). Conformational dynamics of SARS-CoV-2 trimeric spike glycoprotein in complex with receptor ACE2 revealed by cryo-EM. *Sci Adv* 7. [10.1126/sciadv.abe5575](https://doi.org/10.1126/sciadv.abe5575).
103. Lemmin, T., Kalbermatter, D., Harder, D., Plattet, P., and Fotiadis, D. (2020). Structures and dynamics of the novel S1/S2 protease cleavage site loop of the SARS-CoV-2 spike glycoprotein. *J Struct Biol X* 4, 100038. [10.1016/j.jysbx.2020.100038](https://doi.org/10.1016/j.jysbx.2020.100038).

104. Zhang, L., Jackson, C.B., Mou, H., Ojha, A., Peng, H., Quinlan, B.D., Rangarajan, E.S., Pan, A., Vanderheiden, A., Suthar, M.S., et al. (2020). SARS-CoV-2 spike-protein D614G mutation increases virion spike density and infectivity. *Nat Commun* *11*, 6013. 10.1038/s41467-020-19808-4.
105. Daniloski, Z., Jordan, T.X., Ilmain, J.K., Guo, X., Bhabha, G., tenOever, B.R., and Sanjana, N.E. (2021). The Spike D614G mutation increases SARS-CoV-2 infection of multiple human cell types. *Elife* *10*. 10.7554/eLife.65365.
106. Plante, J.A., Liu, Y., Liu, J., Xia, H., Johnson, B.A., Lokugamage, K.G., Zhang, X., Muruato, A.E., Zou, J., Fontes-Garfias, C.R., et al. (2021). Spike mutation D614G alters SARS-CoV-2 fitness. *Nature* *592*, 116-121. 10.1038/s41586-020-2895-3.
107. Zhang, J., Cai, Y., Xiao, T., Lu, J., Peng, H., Sterling, S.M., Walsh, R.M., Jr., Rits-Volloch, S., Zhu, H., Woosley, A.N., et al. (2021). Structural impact on SARS-CoV-2 spike protein by D614G substitution. *Science* *372*, 525-530. 10.1126/science.abf2303.
108. Benton, D.J., Wrobel, A.G., Xu, P., Roustan, C., Martin, S.R., Rosenthal, P.B., Skehel, J.J., and Gamblin, S.J. (2020). Receptor binding and priming of the spike protein of SARS-CoV-2 for membrane fusion. *Nature* *588*, 327-330. 10.1038/s41586-020-2772-0.
109. Benton, D.J., Wrobel, A.G., Borg, A., Xu, P., Martin, S.R., Rosenthal, P.B., Skehel, J.J., and Gamblin, S.J. (2021). The effect of the D614G substitution on the structure of the spike glycoprotein of SARS-CoV-2. *Proc Natl Acad Sci U S A* *118*. 10.1073/pnas.2022586118.
110. Juraszek, J., Rutten, L., Blokland, S., Bouchier, P., Voorzaat, R., Ritschel, T., Bakkers, M.J.G., Renault, L.L.R., and Langedijk, J.P.M. (2021). Stabilizing the closed SARS-CoV-2 spike trimer. *Nat Commun* *12*, 244. 10.1038/s41467-020-20321-x.
111. Yurkovetskiy, L., Wang, X., Pascal, K.E., Tomkins-Tinch, C., Nyalile, T.P., Wang, Y., Baum, A., Diehl, W.E., Dauphin, A., Carbone, C., et al. (2020). Structural and Functional Analysis of the D614G SARS-CoV-2 Spike Protein Variant. *Cell* *183*, 739-751.e738. 10.1016/j.cell.2020.09.032.
112. Wang, D., Zhou, B., Keppel, T.R., Solano, M., Baudys, J., Goldstein, J., Finn, M.G., Fan, X., Chapman, A.P., Bundy, J.L., et al. (2021). N-glycosylation profiles of the SARS-CoV-2 spike D614G mutant and its ancestral protein characterized by advanced mass spectrometry. *Sci Rep* *11*, 23561. 10.1038/s41598-021-02904-w.
113. Hu, J., He, C.-L., Gao, Q.-Z., Zhang, G.-J., Cao, X.-X., Long, Q.-X., Deng, H.-J., Huang, L.-Y., Chen, J., Wang, K., et al. (2020). D614G mutation of SARS-CoV-2 spike protein enhances viral infectivity. *bioRxiv*, 2020.2006.2020.161323. 10.1101/2020.06.20.161323.
114. Li, Q., Wu, J., Nie, J., Zhang, L., Hao, H., Liu, S., Zhao, C., Zhang, Q., Liu, H., Nie, L., et al. (2020). The Impact of Mutations in SARS-CoV-2 Spike on Viral Infectivity and Antigenicity. *Cell* *182*, 1284-1294.e1289. 10.1016/j.cell.2020.07.012.
115. Shajahan, A., Pepi, L., Kumar, B., Murray, N., and Azadi, P. (2022). Site Specific N- and O-glycosylation mapping of the Spike Proteins of SARS-CoV-2 Variants of Concern. *Res Sq*. 10.21203/rs.3.rs-2188138/v1.
116. Gao, C., Zeng, J., Jia, N., Stavenhagen, K., Matsumoto, Y., Zhang, H., Li, J., Hume, A.J., Mühlberger, E., van Die, I., et al. (2020). SARS-CoV-2 Spike Protein Interacts with Multiple Innate Immune Receptors. *bioRxiv*. 10.1101/2020.07.29.227462.
117. Hikmet, F., Méar, L., Edvinsson, Å., Micke, P., Uhlén, M., and Lindskog, C. (2020). The protein expression profile of ACE2 in human tissues. *Mol Syst Biol* *16*, e9610. 10.15252/msb.20209610.
118. Wu, C.Y., Cheng, C.W., Kung, C.C., Liao, K.S., Jan, J.T., Ma, C., and Wong, C.H. (2022). Glycosite-deleted mRNA of SARS-CoV-2 spike protein as a broad-spectrum vaccine. *Proc Natl Acad Sci U S A* *119*. 10.1073/pnas.2119995119.
119. Huang, H.C., Lai, Y.J., Liao, C.C., Yang, W.F., Huang, K.B., Lee, I.J., Chou, W.C., Wang, S.H., Wang, L.H., Hsu, J.M., et al. (2021). Targeting conserved N-glycosylation blocks SARS-CoV-2 variant infection in vitro. *EBioMedicine* *74*, 103712. 10.1016/j.ebiom.2021.103712.
120. van den Elsen, J.M., Kuntz, D.A., and Rose, D.R. (2001). Structure of Golgi alpha-mannosidase II: a target for inhibition of growth and metastasis of cancer cells. *Embo j* *20*, 3008-3017. 10.1093/emboj/20.12.3008.
121. Vallee, F., Karaveg, K., Herscovics, A., Moremen, K.W., and Howell, P.L. (2000). Structural basis for catalysis and inhibition of N-glycan processing class I alpha 1,2-mannosidases. *J Biol Chem* *275*, 41287-41298. 10.1074/jbc.M006927200.
122. Tempel, W., Karaveg, K., Liu, Z.J., Rose, J., Wang, B.C., and Moremen, K.W. (2004). Structure of mouse Golgi alpha-mannosidase IA reveals the molecular basis for substrate specificity among class I (family 47 glycosylhydrolase) alpha1,2-mannosidases. *J Biol Chem* *279*, 29774-29786. 10.1074/jbc.M403065200.

123. Harduin-Lepers, A., Vallejo-Ruiz, V., Krzewinski-Recchi, M.A., Samyn-Petit, B., Julien, S., and Delannoy, P. (2001). The human sialyltransferase family. *Biochimie* 83, 727-737. 10.1016/s0300-9084(01)01301-3.
124. de Vries, T., Knegtel, R.M., Holmes, E.H., and Macher, B.A. (2001). Fucosyltransferases: structure/function studies. *Glycobiology* 11, 119r-128r. 10.1093/glycob/11.10.119r.
125. Peacock, T.P., Goldhill, D.H., Zhou, J., Baillon, L., Frise, R., Swann, O.C., Kugathasan, R., Penn, R., Brown, J.C., Sanchez-David, R.Y., et al. (2021). The furin cleavage site in the SARS-CoV-2 spike protein is required for transmission in ferrets. *Nat Microbiol* 6, 899-909. 10.1038/s41564-021-00908-w.
126. Bagdonaitė, I., Thompson, A.J., Wang, X., Søgaaard, M., Fougeroux, C., Frank, M., Diedrich, J.K., Yates, J.R., 3rd, Salanti, A., Vakhrushev, S.Y., et al. (2021). Site-Specific O-Glycosylation Analysis of SARS-CoV-2 Spike Protein Produced in Insect and Human Cells. *Viruses* 13. 10.3390/v13040551.
127. Tian, W., Li, D., Zhang, N., Bai, G., Yuan, K., Xiao, H., Gao, F., Chen, Y., Wong, C.C.L., and Gao, G.F. (2021). O-glycosylation pattern of the SARS-CoV-2 spike protein reveals an "O-Follow-N" rule. *Cell Res* 31, 1123-1125. 10.1038/s41422-021-00545-2.
128. Saito, A., Irie, T., Suzuki, R., Maemura, T., Nasser, H., Uriu, K., Kosugi, Y., Shirakawa, K., Sadamasu, K., Kimura, I., et al. (2022). Enhanced fusogenicity and pathogenicity of SARS-CoV-2 Delta P681R mutation. *Nature* 602, 300-306. 10.1038/s41586-021-04266-9.
129. Lubinski, B., Frazier, L.E., Phan, M.V.T., Bugembe, D.L., Cunningham, J.L., Tang, T., Daniel, S., Cotten, M., Jaimes, J.A., and Whittaker, G.R. (2022). Spike Protein Cleavage-Activation in the Context of the SARS-CoV-2 P681R Mutation: an Analysis from Its First Appearance in Lineage A.23.1 Identified in Uganda. *Microbiol Spectr* 10, e0151422. 10.1128/spectrum.01514-22.
130. Ghorbani, M., Brooks, B.R., and Klauda, J.B. (2021). Exploring dynamics and network analysis of spike glycoprotein of SARS-COV-2. *Biophys J* 120, 2902-2913. 10.1016/j.bpj.2021.02.047.
131. Lu, Q., Liu, J., Zhao, S., Gomez Castro, M.F., Laurent-Rolle, M., Dong, J., Ran, X., Damani-Yokota, P., Tang, H., Karakousi, T., et al. (2021). SARS-CoV-2 exacerbates proinflammatory responses in myeloid cells through C-type lectin receptors and Tweety family member 2. *Immunity* 54, 1304-1319.e1309. 10.1016/j.immuni.2021.05.006.
132. Suloway, C., Pulokas, J., Fellmann, D., Cheng, A., Guerra, F., Quispe, J., Stagg, S., Potter, C.S., and Carragher, B. (2005). Automated molecular microscopy: the new Legimon system. *J Struct Biol* 151, 41-60. 10.1016/j.jsb.2005.03.010.
133. Lander, G.C., Stagg, S.M., Voss, N.R., Cheng, A., Fellmann, D., Pulokas, J., Yoshioka, C., Irving, C., Mulder, A., Lau, P.W., et al. (2009). Appion: an integrated, database-driven pipeline to facilitate EM image processing. *J Struct Biol* 166, 95-102. 10.1016/j.jsb.2009.01.002.
134. Scheres, S.H. (2012). RELION: implementation of a Bayesian approach to cryo-EM structure determination. *J Struct Biol* 180, 519-530. 10.1016/j.jsb.2012.09.006.
135. He, L., Diedrich, J., Chu, Y.Y., and Yates, J.R., 3rd (2015). Extracting Accurate Precursor Information for Tandem Mass Spectra by RawConverter. *Anal Chem* 87, 11361-11367. 10.1021/acs.analchem.5b02721.
136. Xu, T., Park, S.K., Venable, J.D., Wohlschlegel, J.A., Diedrich, J.K., Cociorva, D., Lu, B., Liao, L., Hewel, J., Han, X., et al. (2015). ProLuCID: An improved SEQUEST-like algorithm with enhanced sensitivity and specificity. *J Proteomics* 129, 16-24. 10.1016/j.jprot.2015.07.001.
137. Tabb, D.L., McDonald, W.H., and Yates, J.R., 3rd (2002). DTASelect and Contrast: tools for assembling and comparing protein identifications from shotgun proteomics. *J Proteome Res* 1, 21-26. 10.1021/pr015504q.
138. Peng, J., Elias, J.E., Thoreen, C.C., Licklider, L.J., and Gygi, S.P. (2003). Evaluation of multidimensional chromatography coupled with tandem mass spectrometry (LC/LC-MS/MS) for large-scale protein analysis: the yeast proteome. *J Proteome Res* 2, 43-50. 10.1021/pr025556v.
139. Park, S.K., Venable, J.D., Xu, T., and Yates, J.R., 3rd (2008). A quantitative analysis software tool for mass spectrometry-based proteomics. *Nat Methods* 5, 319-322. 10.1038/nmeth.1195.
140. Seabright, G.E., Cottrell, C.A., van Gils, M.J., D'Addabbo, A., Harvey, D.J., Behrens, A.J., Allen, J.D., Watanabe, Y., Scaringi, N., Polveroni, T.M., et al. (2020). Networks of HIV-1 Envelope Glycans Maintain Antibody Epitopes in the Face of Glycan Additions and Deletions. *Structure* 28, 897-909.e896. 10.1016/j.str.2020.04.022.
141. Virtanen, P., Gommers, R., Oliphant, T.E., Haberland, M., Reddy, T., Cournapeau, D., Burovski, E., Peterson, P., Weckesser, W., Bright, J., et al. (2020). SciPy 1.0: fundamental algorithms for scientific computing in Python. *Nat Methods* 17, 261-272. 10.1038/s41592-019-0686-2.

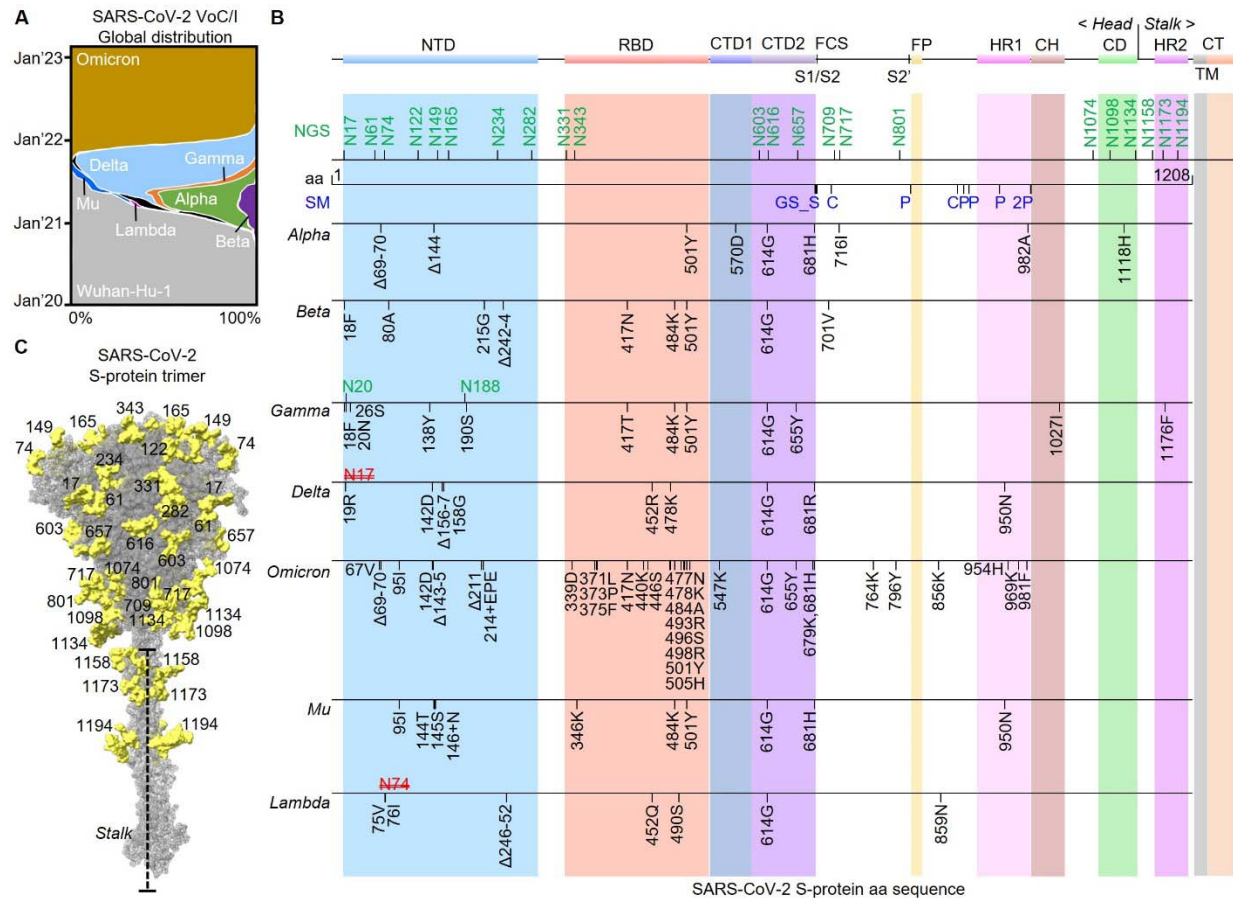


Figure 1: Mutational landscape of spike-protein from SARS-CoV-2 variants. (A) Global waves of SARS-CoV-2 variants over last 3 years and their temporal proportions (modified from nextstrain.org). (B) Critical domains along the amino acid (aa) length of spike-protein *viz.*, N-terminal domain (NTD), Receptor-binding domain (RBD), C-terminal domains (CTD-1 and 2) of S1-protein, Fusion peptide (FP), Heptad repeats (HR-1 and 2), Central helix (CH), Connecting domain (CD), Transmembrane (TM) domain and Cytoplasmic tail (CT), with associated *N*-glycosylation sites (NGS, green), incorporated stabilizing mutations (SM, blue) and most frequent variant-specific mutations (deleted NGS in red). Furin cleavage site (FCS or S1/S2) and the subsequent cleavage site (S2') for other cellular proteases is shown. (C) Structure of the full-length spike-protein trimer with representative *N*-glycans in yellow.

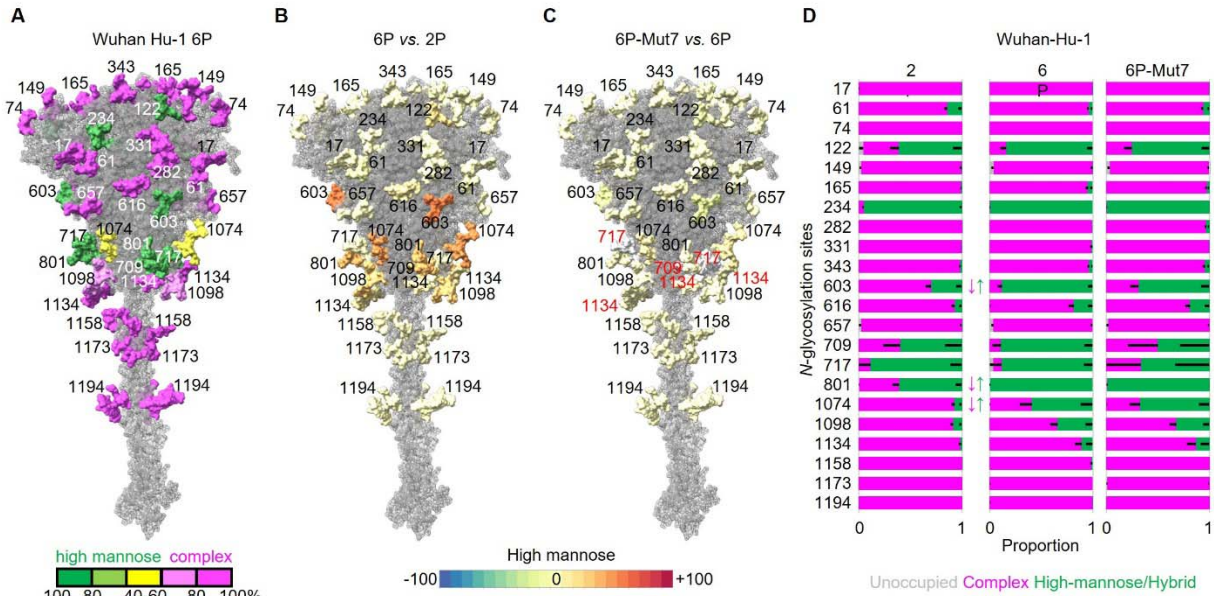


Figure 2: Comparing glycosylation changes on Wuhan-Hu-1 spike-protein owing to stabilizing mutations. (A) *N*-glycan heterogeneity determined on 6P version with dominant proportion color-coded from high mannose (green) to complex (magenta). A percentage-point scale signifying increase (towards red) or decrease (towards blue) in high mannose *N*-glycans, when performing site-specific comparison between 6P and 2P (B), showing significantly reduced *N*-glycan processing at N603, N801 and N1074; and 6P-Mut7 and 6P (C), showing no significant site-specific changes (Poor sampling of peptides mapping N709, N717 and N1134 in 6P-Mut7, numbered in red). (D) Bar-graphs demonstrating site-specific differences in glycosylation, if any, between 3 differently-stabilized mutants. *N*-glycosylation states are color-coded. Error bars represent mean–SEM. Any significant difference (BH-corrected p-value <0.05) in proportion of a certain *N*-glycosylation state at an NGS is represented by color-coded \updownarrow .

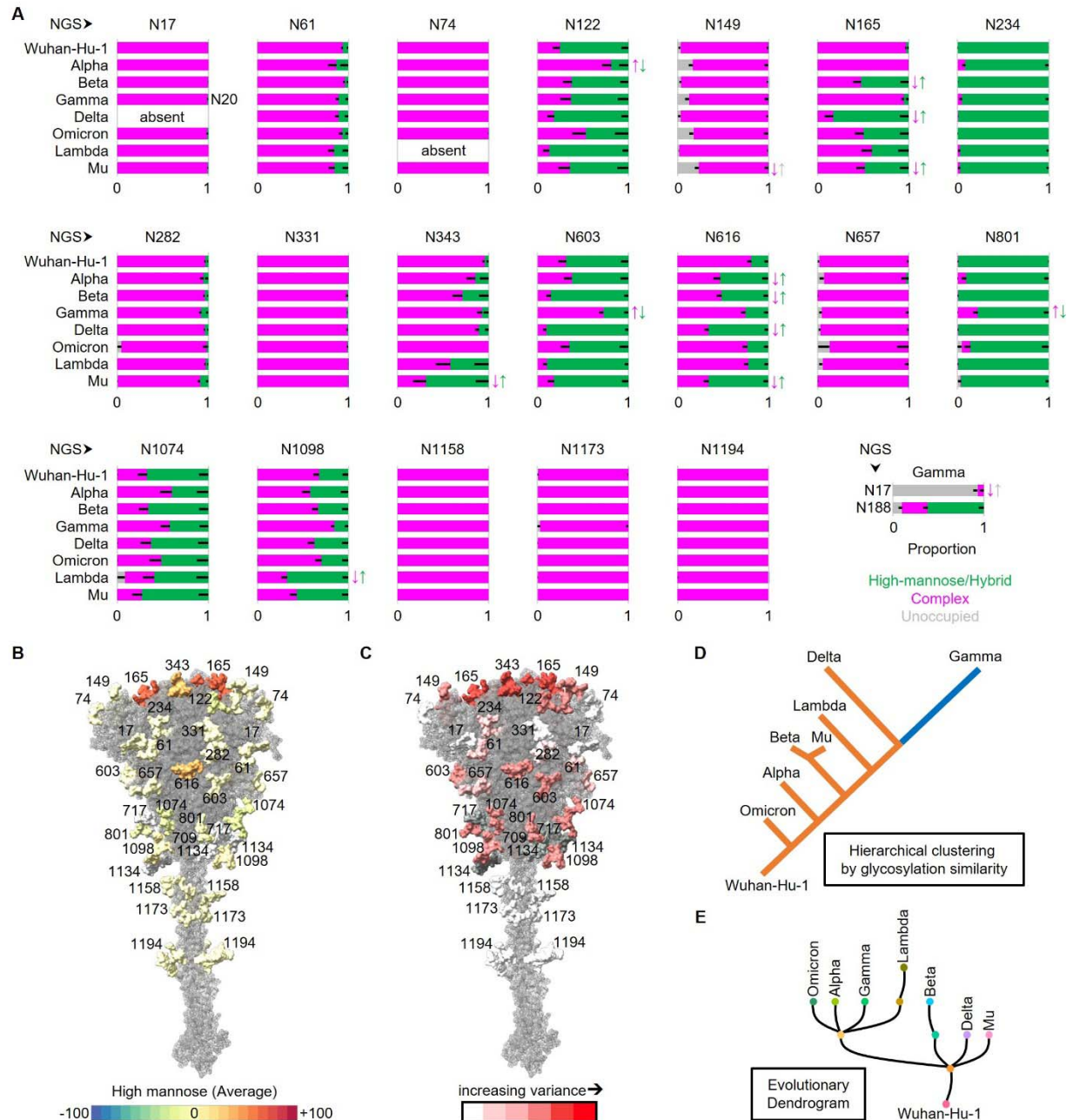


Figure 3: Site-specific comparison of SARS-CoV-2 6P-Mut7 spike-protein trimer from VoC/I with Wuhan-Hu-1. (A) Bar-graphs demonstrating site-specific differences in glycosylation, if any. N17 (glycosylation pattern transferred to N20 in Gamma), N61, N74, N149, N282, N331, N657, N1158, N1173 and N1194 are consistently occupied with mostly complex *N*-glycans across all variants (N17 and N74 absent in Delta and Lambda, respectively). N188 (only in Gamma), N234 and N801 are consistently occupied with mostly high mannose *N*-glycans across all variants. Across all variants, N1074 and N1098 are occupied by a more “even” distribution of high mannose and complex *N*-glycans. Variant specific changes in glycosylation pattern are most apparent at N122, N165, N343, N603 and N616. Across variants, NGS are mostly occupied with *N*-glycans. *N*-glycosylation states are color-coded. Error bars represent mean±SEM. Any significant difference (BH-corrected *p*-value <0.05) in proportion of a certain *N*-glycosylation state at an NGS, compared to the corresponding state in Wuhan-Hu-1, is represented by color-coded ↑. (B) A percentage-point scale signifying increase (towards red) or decrease (towards blue) in high mannose *N*-glycans, averaging across all variants, at each NGS, demonstrating highest shifts at

N165, N343 and N616. (C) Variance in glycosylation state across all variants and Wuhan-Hu-1, with highest variance seen at N165 and N343. (D) Hierarchical clustering of SARS-CoV-2 variants and Wuhan-Hu-1 by similarity in glycosylation state shows Omicron is most similar to Wuhan-Hu-1, and Gamma and Delta the most dissimilar. (E) An evolutionary dendrogram of SARS-CoV-2 variants based on GISAID data considering nucleic acid mutations (covariants.org). None of the above analyses consider N709, N717 and N1134 owing to inconsistent sampling.

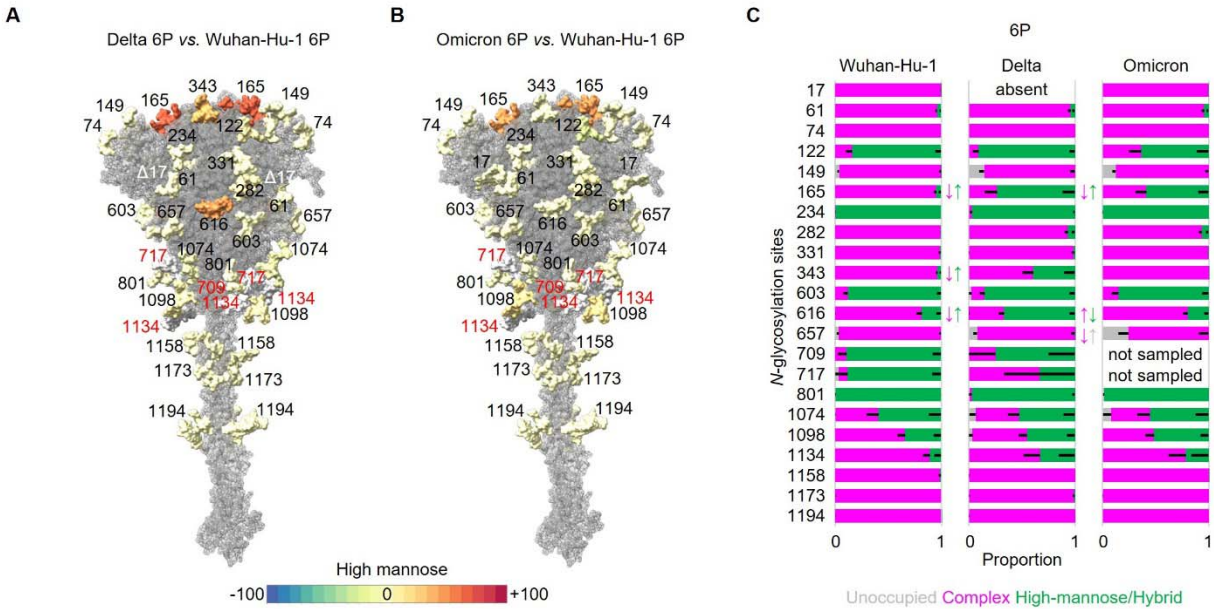


Figure 4: Site-specific comparison of SARS-CoV-2 6P spike-protein trimer from Wuhan-Hu-1, Delta and Omicron. A percentage-point scale signifying increase (towards red) or decrease (towards blue) in high mannose *N*-glycans, when performing site-specific comparison between Delta and Wuhan-Hu-1 (A), showing significantly reduced *N*-glycan processing at N165, N343 and N616; and Omicron and Wuhan-Hu-1 (B), showing prominently reduced *N*-glycan processing at N165, but not statistically significant. (C) Bar-graphs demonstrating site-specific differences in glycosylation, if any, between Wuhan-Hu-1 and Delta, and Delta and Omicron. *N*-glycosylation states are color-coded. Error bars represent mean±SEM. Any significant difference (BH-corrected *p*-value <0.05) in proportion of a certain *N*-glycosylation state at an NGS is represented by color-coded ↓. The significant shift from complex *N*-glycans in Wuhan-Hu-1 to high mannose *N*-glycans in Delta at N165, N343 and N616, reverts from Delta to Omicron.

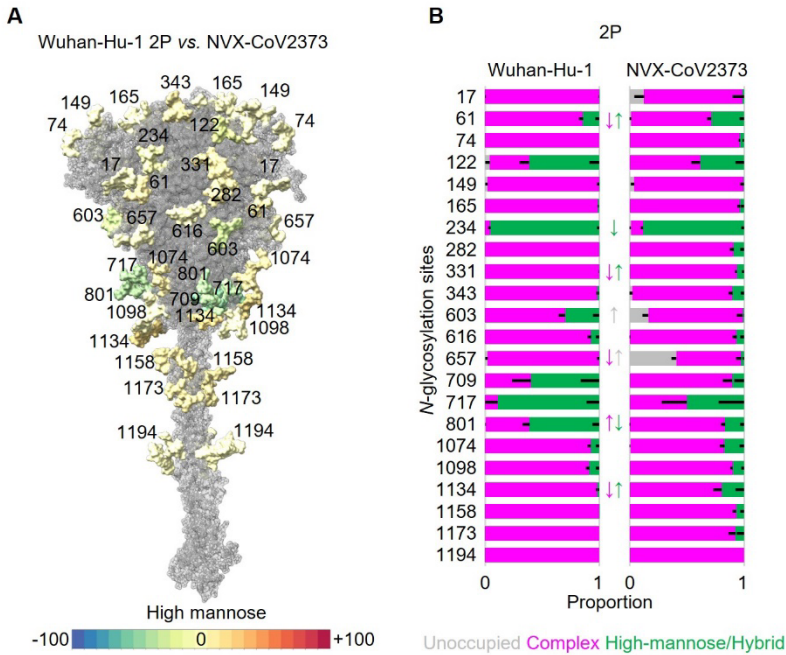


Figure 5: Comparing glycosylation changes between Wuhan-Hu-1 2P spike-protein and NVX-CoV2373. A percentage-point scale signifying increase (towards red) or decrease (towards blue) in high mannose *N*-glycans, shows not much difference between the 2 spike-protein trimers (A), even though many of the smaller differences are significant (B) owing much higher sampling from NVX-CoV2373. *N*-glycosylation states are color-coded. Error bars represent mean–SEM. Any significant difference (BH-corrected *p*-value <0.05) in proportion of a certain *N*-glycosylation state at an NGS is represented by color-coded \updownarrow .